

1 **The control of hydrogen sulfide on benthic iron and**  
2 **cadmium fluxes in the oxygen minimum zone off Peru**

3

4 Anna Plass<sup>1\*</sup>, Christian Schlosser<sup>1</sup>, Stefan Sommer<sup>1</sup>, Andrew W. Dale<sup>1</sup>, Eric P.  
5 Achterberg<sup>1</sup>, Florian Scholz<sup>1\*</sup>

6 <sup>1</sup>GEOMAR Helmholtz Centre for Ocean Research Kiel, Wischhofstraße 1-3, 24148  
7 Kiel, Germany

8 \*Correspondence to: Anna Plass (aplass@geomar.de), Florian Scholz  
9 (fscholz@geomar.de)

10

## 11 **Abstract**

12 Sediments in oxygen-depleted marine environments can be an important sink or  
13 source of bio-essential trace metals in the ocean. However, the key mechanisms  
14 controlling the release from or burial of trace metals in sediments are not exactly  
15 understood. Here, we investigate the benthic biogeochemical cycling of Fe and Cd in  
16 the oxygen minimum zone off Peru. We combine bottom water and pore water  
17 concentrations, as well as benthic fluxes determined from pore water profiles and in-  
18 situ from benthic chamber incubations, along a depth transect at 12° S. In agreement  
19 with previous studies, both concentration-depth profiles and in-situ benthic fluxes  
20 indicate a release of Fe from sediments to the bottom water. Diffusive Fe fluxes and  
21 Fe fluxes from benthic chamber incubations ( $-0.3 - -17.5 \text{ mmol m}^{-2} \text{ y}^{-1}$ ) are broadly  
22 consistent at most stations, indicating that diffusion is the main transport mechanism  
23 of dissolved Fe across the sediment-water interface. The occurrence of mats of sulfur  
24 oxidizing bacteria on the seafloor represents an important control on the spatial  
25 distribution of Fe fluxes by regulating hydrogen sulfide ( $\text{H}_2\text{S}$ ) concentrations and,  
26 potentially, Fe sulfide precipitation within the surface sediment. Rapid removal of  
27 dissolved Fe after its release to anoxic bottom waters hints to oxidative removal by  
28 nitrite and interactions with particles in the near-bottom water column. Benthic flux  
29 estimates of Cd suggest a flux into the sediment within the oxygen minimum zone.  
30 Fluxes from benthic chamber incubations (up to  $22.6 \text{ } \mu\text{mol m}^{-2} \text{ y}^{-1}$ ) exceed diffusive  
31 fluxes ( $< 1 \text{ } \mu\text{mol m}^{-2} \text{ y}^{-1}$ ) by a factor  $> 25$ , indicating that downward diffusion of Cd  
32 across the sediment-water interface is of subordinate importance for Cd removal from  
33 benthic chambers. As Cd removal in benthic chambers co-varies with  $\text{H}_2\text{S}$   
34 concentrations in the pore water of surface sediments, we argue that Cd removal is  
35 mediated by precipitation of CdS within the chamber water or directly at the  
36 sediment-water interface. A mass balance approach, taking into account the  
37 contributions of diffusive and chamber fluxes as well as Cd delivery with organic  
38 material, suggests that CdS precipitation in the near-bottom water could make an  
39 important contribution to the overall Cd mass accumulation in the sediment solid  
40 phase. According to our results, the solubility of trace metal sulfide minerals (Cd  $\ll$   
41 Fe) is a key-factor controlling trace metal removal and consequently the magnitude  
42 as well as the temporal and spatial heterogeneity of sedimentary fluxes. We argue  
43 that depending on their sulfide solubility, sedimentary source or sink fluxes of trace  
44 metals will change differentially as a result of declining oxygen concentrations and an

45 associated expansion of sulfidic surface sediments. Such a trend could cause a  
46 change in the trace metal stoichiometry of upwelling water masses with potential  
47 consequences for marine ecosystems in the surface ocean.

48

49

## 50 **1. Introduction**

51

### 52 **1.1 Scientific rationale**

53 The world's oceans are losing oxygen (e.g. Keeling et al. 2010; Stramma et al.  
54 2010; Helm et al. 2011). In total around 2 % of oxygen has been lost over the past  
55 five decades (Schmidtko et al., 2017) and an expansion of oxygen minimum zones  
56 (OMZs) in the tropical oceans has been documented over the same timespan  
57 (Stramma et al., 2008). The biogeochemical cycling of several nutrient-type trace  
58 metals (TMs) is likely to be particularly susceptible to changing oxygen  
59 concentrations as they occur in different oxidation states (e.g. Fe, Mn, Co) and/or are  
60 precipitated as sulfide mineral in anoxic-sulfidic environments (e.g. Fe, Zn, Cd; listed  
61 in the order of decreasing sulfide solubility). However, with the exception of Fe (Dale  
62 et al., 2015a; Lohan and Bruland, 2008; Rapp et al., 2018; Schlosser et al., 2018;  
63 Scholz et al., 2014a), little information is available on how other TM fluxes will  
64 respond to ocean deoxygenation. As certain TMs are essential for the growth of  
65 marine organisms (e.g. Fe, Mn, Co, Ni, Zn, Cd), TM availability can (co-)limit primary  
66 productivity and therefore affect oceanic carbon sequestration through the biological  
67 pump (Saito et al., 2008; Moore et al., 2013; Morel et al., 2014). As a consequence, a  
68 better understanding of how TMs respond to low oxygen conditions is essential for  
69 predicting how marine ecosystems and the carbon cycle will evolve in the future  
70 ocean, with modelling scenarios predicting a continuation of ocean deoxygenation  
71 (Bopp et al., 2002; Oschlies et al., 2008; Keeling et al., 2010)

72 Marine sediments are an important source or sink of TMs to the ocean under  
73 low oxygen conditions (Böning et al., 2004; Brumsack, 2006; Scor Working Group,  
74 2007; Severmann et al., 2010; Noble et al., 2012; Biller and Bruland, 2013; Conway  
75 and John, 2015b; Klar et al., 2018). In the OMZ off the coast of Peru, substantial

76 fluxes of reduced Fe and other TMs across the sediment-bottom water interface have  
77 been documented (Noffke et al., 2012; Scholz et al., 2016) or inferred (Hawco et al.,  
78 2016). While a number of studies have addressed biogeochemical processes that  
79 lead to benthic Fe release, the key biogeochemical processes and conditions that  
80 control the sedimentary release or burial of other TMs in open marine systems are  
81 still poorly constrained. Moreover, a detailed picture of removal or stabilization  
82 processes and rates that take place in the highly dynamic water layer overlying the  
83 seafloor is lacking.

84 In this article, we compare the benthic biogeochemical cycling of Fe and Cd. It  
85 has been established that the Peruvian OMZ represents a source of dissolved Fe to  
86 the ocean (Noffke et al., 2012; Fitzsimmons et al., 2016; John et al., 2018). In  
87 contrast, earlier studies have demonstrated that OMZs represent a sink for Cd  
88 (Janssen et al., 2014; Böning et al., 2004). Because of their contrasting tendency to  
89 form sulfide minerals and different supply pathways to the sediment, Fe and Cd can  
90 serve as prototypes to provide information about how sedimentary fluxes of different  
91 TMs may respond to declining oxygen concentrations. Under more reducing  
92 conditions the mobility of TMs can either be enhanced or diminished, e.g., through  
93 precipitation of sulfide minerals that are buried in the sediments (e.g. Westerlund et  
94 al., 1986; Rigaud et al., 2013; Olson et al., 2017). Increased burial or release of TMs  
95 at the seafloor can have an impact on the amplitude of primary productivity,  
96 especially at the eastern ocean boundaries where the near-bottom water column is  
97 connected to the surface ocean via upwelling. Moreover, since the inventories of TMs  
98 in the ocean are generally dependent on the respective input and output fluxes,  
99 changes in the balance between trace metal recycling and burial can have an impact  
100 on oceanic TM reservoirs on longer timescales. By comparing the benthic  
101 biogeochemical cycling of Fe and Cd across spatial and temporal redox gradients,  
102 we aim to provide general constraints on how the stoichiometry of bio-essential TMs  
103 in seawater may be affected by ocean deoxygenation.

104

## 105 **1.2. Marine biogeochemistry of iron**

106 Iron is the most abundant TM in phytoplankton and part of a range of  
107 metalloenzymes that are involved in important biological functions, such as  
108 photosynthesis or nitrogen fixation (Twining and Baines, 2013). Despite Fe being

109 highly abundant in the continental crust, its low availability limits primary productivity  
110 in up to 30 % of the surface ocean area (Moore et al., 2013). This limitation arises  
111 from the low solubility of its thermodynamically stable form in oxic waters, Fe(III).  
112 Concentrations can reach up to ~ 1 nM when Fe(III) is kept in solution through  
113 complexation with organic ligands (Rue and Bruland, 1997; Liu and Millero, 2002;  
114 Boyd and Ellwood, 2010; Raiswell and Canfield, 2012). The thermodynamically  
115 stable form of Fe under anoxic conditions, Fe(II), is more soluble and therefore  
116 anoxic waters are typically characterized by higher dissolved Fe concentrations (up  
117 to tens of nM) (Conway and John, 2014; Vedamati et al., 2014; Fitzsimmons et al.,  
118 2016; Schlosser et al., 2018).

119 Sediments within OMZs are considered an important source of dissolved Fe  
120 and some of the highest sedimentary Fe fluxes have been observed in these regions  
121 (Severmann et al., 2010; Noffke et al., 2012). Under anoxic conditions, Fe(II) can be  
122 liberated from the sediments into pore waters from Fe-(oxyhydr)oxides through  
123 reductive dissolution by microbes or abiotic reduction with H<sub>2</sub>S (Canfield, 1989). In  
124 the absence of oxygen, dissolved Fe(II) escapes the rapid re-oxidation and  
125 subsequent (oxyhydr)oxide precipitation and can, therefore, diffuse from pore waters  
126 into bottom waters. However, in anoxic OMZs, where denitrification takes place,  
127 Fe(II) can also be re-oxidized with nitrate as a terminal electron acceptor, either  
128 mediated by nitrate-reducing microbes or abiotically through reaction with nitrite  
129 (Straub et al., 1996; Carlson et al., 2013; Scholz et al., 2016; Heller et al., 2017). The  
130 solubility of Fe in sulfidic (i.e. NO<sub>3</sub><sup>-</sup> and NO<sub>2</sub><sup>-</sup> depleted) water is relatively high  
131 (Rickard et al., 2006) and during sulfidic events dissolved Fe can accumulate in the  
132 water column (up to hundreds of nM) because of decreased Fe oxidation (Scholz et  
133 al., 2016) and stabilization as aqueous Fe sulfide complexes and clusters (Schlosser  
134 et al., 2018). However, Fe fluxes across the benthic boundary have also been  
135 hypothesized to decrease under strongly sulfidic conditions in the surface sediments,  
136 when pore waters become oversaturated with respect to Fe monosulfide (Scholz et  
137 al., 2014), which is the precursor for pyrite (FeS<sub>2</sub>) (Raiswell and Canfield, 2012).

138

### 139 **1.3. Marine biogeochemistry of cadmium**

140 Cd is abundant in phytoplankton despite concentrations that are one order of  
141 magnitude lower than Fe (Moore et al., 2013; Twining and Baines, 2013). A function

142 for Cd as a catalytic metal atom in the carbonic anhydrase protein has been found in  
143 diatoms (Lane and Morel, 2000) and it can also substitute Zn and enhance  
144 phytoplankton growth under Zn limitation in different phytoplankton species (Price  
145 and Morel, 1990; Lee and Morel, 1995; Sunda and Huntsman, 2000; Xu et al., 2008).  
146 In marine sediments Cd can be released from the solid phase to the pore waters  
147 through the remineralization of organic matter (Klinkhammer et al., 1982; Collier and  
148 Edmond, 1984; Gendron et al., 1986; Gerringa, 1990; Audry et al., 2006; Scholz and  
149 Neumann, 2007). After its release to the pore water, Cd can diffuse across the  
150 sediment-water interface. Under anoxic and sulfidic conditions, Cd is thought to be  
151 precipitated as CdS (Greenockite) and retained in the sediment (Westerlund et al.,  
152 1986; Gobeil et al., 1987; Rosenthal et al., 1995; Audry et al., 2006). Due to its low  
153 sulfide solubility, CdS can precipitate at much lower H<sub>2</sub>S concentrations than FeS  
154 (mackinawite) (Morse and Luther, 1999).

155 Most previous studies have focused on the benthic cycling of Cd in near- and  
156 in-shore environments such as estuaries and lagoons (e.g. Westerlund et al., 1986;  
157 Colbert et al., 2001; Audry et al., 2006b; Metzger et al., 2007; Point et al., 2007;  
158 Scholz and Neumann, 2007). By contrast, little is known about Cd cycling in open-  
159 marine sedimentary environments, where the redox- and sediment-dynamics are  
160 different. Previous studies on sedimentary Cd cycling generally concluded that the  
161 flux of organic material and the presence of H<sub>2</sub>S are the most important factors  
162 controlling the balance between Cd recycling versus precipitation and burial (e.g.  
163 Westerlund et al., 1986; Colbert et al., 2001; Audry et al., 2006; Metzger et al., 2007;  
164 Scholz and Neumann, 2007). Low oxygen regions in the ocean are considered an  
165 important sink for Cd (Janssen et al., 2014; Conway and John, 2015a; Xie et al.,  
166 2019) and sediments below OMZs are highly enriched in Cd (Ragueneau et al.,  
167 2000; Böning et al., 2004; Borchers et al., 2005; Muñoz et al., 2012; Little et al.,  
168 2015). However, the respective contributions of different Cd removal mechanisms to  
169 Cd accumulation in the sediment have not been quantified.

170

#### 171 **1.4. Study area**

172 Seasonal upwelling of nutrient-rich waters off the Peruvian coast in austral  
173 winter leads to high rates of primary productivity in the photic zone ( $\sim 300 \text{ mmol C m}^{-3}$   
174  $\text{d}^{-1}$ ) (Pennington et al., 2006). The combination of oxygen consumption through the

175 respiration of this organic matter and low oxygen concentrations in water masses that  
176 supply upwelling regions, leads to the formation of one of the world's most intense  
177 OMZs, with complete oxygen consumption in the OMZ core between ~ 100 m – 300  
178 m water depth (Karstensen et al., 2008; Thamdrup et al., 2012). Upon oxygen  
179 depletion,  $\text{NO}_3^-$  can serve as an electron acceptor for respiration. Therefore,  
180 denitrification, dissimilatory reduction of  $\text{NO}_3^-$  to ammonium (DNRA) and anaerobic  
181 ammonium oxidation (anammox) with  $\text{NO}_2^-$  are important biogeochemical processes  
182 within the anoxic and nitrogenous water column (Lam et al., 2009; Lam and Kuypers,  
183 2011; Dalsgaard et al., 2012). The OMZ overlying the Peruvian shelf is a temporally  
184 and spatially dynamic system where biogeochemical conditions can range from fully  
185 oxic to anoxic and sulfidic. Occasional shelf oxygenation events occur mostly during  
186 El Niño events and are linked to the propagation of coastal trapped waves (Gutiérrez  
187 et al., 2008). During such events, oxygenated water can be found on the upper slope  
188 to 200 m – 300 m water depth (Levin et al., 2002). By contrast, sulfidic events can  
189 occur during periods of stagnation, when oxygen,  $\text{NO}_3^-$  and  $\text{NO}_2^-$  become depleted in  
190 the water column due to sluggish ventilation. Once  $\text{NO}_3^-$  and  $\text{NO}_2^-$  are depleted,  
191 chemolithoautotrophic  $\text{H}_2\text{S}$  oxidation is impeded. Hydrogen sulfide produced by  
192 bacterial sulfate reduction in sediments can then be released to the water column  
193 (Schunck et al., 2013) at rates reaching several  $\text{mmol m}^{-2} \text{d}^{-1}$  (Sommer et al., 2016).

194 Our sampling campaign (cruises M136 and M137) took place in April and May  
195 2017, during the decline of a coastal El Niño event. A coastal El Niño is a local  
196 phenomenon that refers to reduced upwelling and increased sea surface  
197 temperatures off the coasts of Peru and Ecuador, with typically heavy rainfall on land.  
198 During this event in austral summer, coastal waters off Peru showed a strong positive  
199 sea surface temperature anomaly of up to 2 to 4 °C (Echevin et al., 2018; Garreaud,  
200 2018). The warming is proposed to be a result of strong local alongshore wind  
201 anomalies and equatorial Kelvin waves propagating towards the Peruvian coast  
202 (Echevin et al., 2018; Peng et al., 2019).

203

204

## 205 **2. Methods**

206

## 207 **2.1 Sampling and sample handling**

208 In this study, data from three different types of samples were combined: (1)  
209 pore waters for the determination of benthic diffusive fluxes and to study TM cycling  
210 in sediments; (2) Benthic chamber incubations, to determine in-situ fluxes across the  
211 sediment-water interface; (3) Bottom water concentration-depth profiles to determine  
212 the fate of TMs in the particle-rich and dynamic near-bottom water column.

213 The sampling took place during RV Meteor cruises M136 and M137 in austral  
214 autumn between April and May 2017. We also compared our data to benthic diffusive  
215 Fe(II) fluxes from RV Meteor cruise M92 that took place in austral summer during  
216 January 2013. Our sampling stations covered the entire Peruvian shelf and slope  
217 across a transect at 12°S (Fig. 1) with water depths from 75 – to 950 m, thus  
218 including stations above, inside and below the permanent OMZ. Our sampling of pore  
219 waters and sample collection from benthic chamber incubations generally followed  
220 the methodology described in Noffke et al. (2012).

221 Short sediment cores of 30 – 40 cm length were retrieved with a multiple corer  
222 (MUC). Upon recovery, the cores were directly transferred into the ship's cool room  
223 (4°C). The supernatant bottom water was instantly sampled and filtered through 0.2  
224 µm cellulose acetate filters (Sartorius) and acidified to pH < 1 with subboiled distilled  
225 HNO<sub>3</sub>. The sediment cores were subsequently sampled in vertical sections in a glove  
226 bag under Ar atmosphere to prevent any contact with oxygen. The sediment samples  
227 were centrifuged to separate the pore waters from the sediment solid phase. Pore  
228 waters were then filtered in another Ar-filled glove bag through 0.2 µm cellulose  
229 acetate filters (Sartorius). An 8 ml aliquot was acidified to pH < 1 with subboiled  
230 distilled HNO<sub>3</sub> and stored in acid cleaned low-density polyethylene (LDPE) bottles for  
231 TM analysis. Another aliquot was taken for analysis of H<sub>2</sub>S concentrations. Additional  
232 sediment subsamples were collected in pre-weighed cups for water content and  
233 porosity determination as well as for Cd and organic C concentrations measurements  
234 in the solid phase.

235 Benthic landers, constructed from titanium frames, containing two circular  
236 benthic chambers for in-situ incubations, were deployed on the seafloor (see  
237 Sommer et al. (2009) for details). After placement of the lander on the seafloor, the  
238 benthic chambers (internal diameter of 28.8 cm) were partially driven into the  
239 sediment, covering a sediment area of 651.4 cm<sup>2</sup>. A volume between 12 – 18 l,



240 overlying the first 20 – 30 cm of the seafloor, was enclosed in the chamber,  
241 depending on the insertion depth of the chamber into the sediment. Prior to the  
242 incubation, the seawater contained in the chamber was repeatedly replaced with  
243 ambient seawater to replace solutes and flush out particles that might have been  
244 mobilized during the insertion of the chamber into the sediment. Over the incubation  
245 time of around 32 hours, 8 consecutive samples of 12 ml were filtered in-situ through  
246 0.2  $\mu\text{m}$  cellulose acetate filters (Sartorius) via peristaltic pumps and collected in  
247 quartz glass tubes. All sampling tubes were acid cleaned prior to use to guarantee a  
248 TM clean sampling. After recovery of the lander, the quartz glass tubes were  
249 transferred to the laboratory and samples were stored in acid cleaned LDPE bottles  
250 and acidified to  $\text{pH} < 2$  with subboiled distilled  $\text{HNO}_3$ . Other samples were collected  
251 simultaneously for analysis of nitrogen species. The incubated sediments within the  
252 benthic chamber were sampled after recovery of the lander and pore waters were  
253 extracted to analyze  $\text{H}_2\text{S}$  concentrations for comparison with pore water profiles from  
254 parallel MUCs.

255 To determine TM concentrations across the near-bottom water column, water  
256 samples were collected at 0.5, 1.0, 2.0, 3.0 and 4.0 m above the seafloor using  
257 sampling apparatus attached to the landers. Filter holders with 0.2  $\mu\text{m}$  polyether  
258 sulfone filters (Supor) were attached at the various depths and connected to  
259 sampling tubes that went through peristaltic pumps into gas sampling bags (Tedlar).  
260 Sampling at 3.0 m and 4.0 m above the seafloor was realized by attaching the filter  
261 holders and tubing to an arm that was automatically unfolded upon placement of the  
262 lander at the seafloor. The peristaltic pumps transferred the seawater from the  
263 sampling depths into the sampling bags over the same time period as the lander  
264 incubations of around 32 hours. This resulted in an average sample volume of 1.5 l  
265 per depth. All filters, tubing and sampling bags were acid cleaned prior to deployment  
266 to guarantee a TM clean sampling. Directly after sample retrieval, an 60 ml aliquot  
267 was stored in acid cleaned LDPE bottles and acidified to  $\text{pH} < 2$  for TM analysis.  
268 Another aliquot was taken for analysis of silicic acid ( $\text{Si}(\text{OH})_4$ ).

269

## 270 **2.2 Analytical methods**

271 Concentrations of Fe(II) in pore waters were measured on board directly after  
272 sample retrieval by photometry using the ferrozine method (Stookey, 1970). Other

273 geochemical parameters in our different samples were also determined photometrical  
274 (U-2001 Hitachi spectrometer) using standard techniques (Grasshoff et al., 1999).  
275 Hydrogen sulfide concentrations were determined using the methylene blue method  
276 and  $\text{Si(OH)}_4$  concentrations were determined using a heptamolybdate solution as  
277 reagent. Concentrations of nitrogen species were determined by an auto-analyzer  
278 (QuAAtro, SEAL Analytical) using sulfanilamide as reagent (Hydes et al., 2010).

279 For TM analysis of bottom water samples we followed the procedure described  
280 by Rapp et al. (2017), whereby the TMs were pre-concentrated by a fully automated  
281 device (SeaFAST). After raising the sample pH to 6.4 with an ammonium acetate  
282 buffer (1.5 M), 15 ml of sample was loaded onto a chelating resin column, where the  
283 seawater matrix was rinsed off, before the TMs were collected into 1 ml elution acid (1  
284 M subboiled  $\text{HNO}_3$ ). Due to the smaller size of pore water samples and samples from  
285 benthic lander incubations, a half-automated device (Preblab) with a smaller sample  
286 loop and thus dead volume was used. On this device, sample loading and collection  
287 as well as the addition of buffer was done manually. For samples from benthic lander  
288 incubations and pore waters, an amount of 3 ml and 1 ml, respectively, was needed  
289 for pre-concentration. The samples were diluted with de-ionised water (MilliQ,  
290 Millipore) to increase the sample volume to 5 ml for samples from benthic chamber  
291 incubations and to 3 ml for pore waters. The pre-concentrated samples were  
292 measured by ICP-MS (HR-ICP-MS; Thermo Fisher Element XR) and TM  
293 concentrations were quantified by isotope dilution. The detection limits were 28.8 pM  
294 for Fe and 0.8 pM for Cd (Rapp et al., 2017). Accuracies for replicate measurements  
295 of reference seawater certified for TMs are listed in Table 1.

296 For the calculation of sedimentary Cd enrichments ( $\text{Cd}_{\text{xs}}$ ), Cd and Al contents  
297 in sediments were determined following total digestions of freeze dried and ground  
298 sediment samples. The sediment was digested in 40 % HF (suprapure), 65 %  $\text{HNO}_3$   
299 (suprapure) and 60 %  $\text{HClO}_4$  (suprapure). Concentrations were measured by ICP-  
300 OES (VARIAN 720-ES). The reference standard MESS was used to check the  
301 digestion procedure. The accuracy was  $\pm 0.3$  % for Cd and  $\pm 1.3$  % for Al (MESS-3  
302 Cd:  $0.24 \pm 0.01 \mu\text{g g}^{-1}$ , recommended value  $0.24 \pm 0.01 \mu\text{g g}^{-1}$ , MESS-3 Al:  $8.59 \pm$   
303  $0.11 \mu\text{g g}^{-1}$ , recommended value  $8.59 \pm 0.23 \mu\text{g g}^{-1}$ ).

304 Organic carbon content in the sediment was determined using an Elemental  
305 Analyzer (Euro EA) after removal of inorganic carbon with 0.25 mM HCl. Precision of  
306 the measurement was  $\pm 1$  %.

307

### 308 **2.3 Diffusive flux calculations**

309 Benthic diffusive fluxes ( $F_D$ ) were determined using Fick's first law of diffusion  
310 using concentration gradients between the uppermost pore water sample (0 – 1 cm)  
311 and the overlying bottom water ( $dC/dx$ ) (Boudreau, 1997):

$$312 \quad F_D = -\Phi D_{sed}(dC/dx) \quad (1)$$

313 The effective molecular diffusion coefficients of Fe and Cd for sediments ( $D_{sed}$ ) were  
314 calculated from the molecular diffusion coefficient in seawater ( $D_{sw}$ ) under standard  
315 conditions (Li and Gregory, 1974) by adjusting it to in-situ temperature, pressure and  
316 salinity applying the Stokes-Einstein Equation. We determined the diffusion  
317 coefficients for sediments as follows:

$$318 \quad D_{sed} = D_{sw}/\theta^2 \quad (2)$$

319 Tortuosity ( $\theta$ ) was calculated from porosity ( $\Phi$ ) as follows (Boudreau, 1997):

$$320 \quad \theta^2 = 1 - \ln(\phi^2) \quad (3)$$

321 Positive values represent a flux from the bottom water into the sediment pore  
322 water, negative values a flux from the sediment pore water into the bottom water. All  
323 input values for the diffusive flux calculations are listed in Tables S1 and S2 in the  
324 supplement.

325 We chose to use the commonly applied approach of a two point concentration  
326 gradient for the determination of diffusive fluxes, as more advanced curve fitting  
327 methods would fail to capture sharp concentration gradients at the sediment surface  
328 and, thus, lead to erroneous flux estimates (Shibamoto and Harada, 2010).

329 The fluxes from benthic lander incubations were calculated from the slopes of  
330 linear regressions from the concentration-time data. The relevant equations are listed  
331 together with the coefficients of determination ( $R^2$ ) in Table S4 in the supplement.  
332 Fluxes were determined using the water volume enclosed in the benthic chamber,

333 estimated for each deployment from the insertion depth of the benthic chamber into  
334 the sediment.

335

336

### 337 **3. Results**

338

#### 339 **3.1 Biogeochemical conditions in the water column**

340 Due to the particular atmospheric and oceanographic conditions, the decline of  
341 a coastal El Niño during our sampling campaign (cruises M136 and M137), the water  
342 column overlying the Peruvian shelf was oxygenated. Oxygen concentrations were >  
343 20  $\mu\text{M}$  in the water column down to around 100 m water depth. However, bottom  
344 water oxygen concentrations directly above the seafloor, measured using optodes  
345 attached to lander, were below the detection limit (> 1  $\mu\text{M}$ ) at the shallowest station  
346 (Station 1). The OMZ, with  $\text{O}_2$  concentrations < 5  $\mu\text{M}$ , extended from around 120 to  
347 400 m water depth. The water column within the OMZ was nitrogenous (i.e.  $\text{NO}_3^-$   
348 reducing) as indicated by the presence of  $\text{NO}_2^-$  ( $\geq 4 \mu\text{M}$ ), an intermediate product of  
349 denitrification (Zumft, 1997). Oxygen gradually increased to > 50  $\mu\text{M}$  below 400 m  
350 towards 950 m water depth (Fig. 2). As we will compare some of our data to those of  
351 an earlier cruise (M92), the corresponding oxygen distribution across the Peruvian  
352 continental margin is shown for comparison (Fig. 2).

353

#### 354 **3.2 Bottom water, pore water and benthic flux data**

355

##### 356 **3.2.1 Iron**

357 Iron concentrations in near-bottom waters decreased from near-shore to off-  
358 shore stations, from > 100 nM at the shallowest shelf station at 75 m water depth  
359 (Station 1) to 6 nM at 750 m water depth (Station 9) (Fig. 3). At a number of stations  
360 within the OMZ (Stations 3 and 4), vertical concentration gradients were observed.  
361 Here Fe concentrations decreased by 15 – 20 nM from 0.5 to 4 m above the seafloor.  
362 Multiple sampling at the shallowest shelf station (Station 1) revealed that Fe

363 concentrations were temporally variable and ranged from ~ 100 nM at the end of  
364 April to < 60 nM at the end of May 2017.

365 Concentrations of Fe(II) in pore waters were highest (up to a few  $\mu\text{M}$ ) in the  
366 upper 5 – 10 cm of the sediment cores. Deeper in the sediment cores, concentrations  
367 decreased to > 0.2  $\mu\text{M}$  (Fig. 4). At all stations, sharp concentration gradients between  
368 the uppermost pore water and bottom water sample were observed, with higher  
369 concentrations in pore waters at the sediment surface ( $\mu\text{M}$ ) than in the overlying  
370 bottom water (nM). This observation implies a diffusive flux from pore waters into  
371 bottom waters. The steepest concentration gradients across the sediment-water  
372 interface were observed within the OMZ. The highest Fe(II) concentrations at the  
373 sediment surface (> 6  $\mu\text{M}$ ) were observed at Station 4 (145 m water depth). At this  
374 station, the benthic diffusive flux into the bottom waters was also highest at -17.5  
375  $\text{mmol m}^{-2} \text{y}^{-1}$ . The lowest diffusive fluxes of 0.0 (due to concentrations below the  
376 detection limit) and -0.3  $\text{mmol m}^{-2} \text{y}^{-1}$  were observed on the upper slope below the  
377 OMZ at Stations 9 and 10 respectively (Table 2). An accumulation of  $\text{H}_2\text{S}$  in pore  
378 waters coincided with a depletion of Fe(II) concentrations (Fig. 4). At Station 1, we  
379 observed the highest  $\text{H}_2\text{S}$  concentrations throughout the core and in particular at the  
380 sediment surface, with maximum concentrations reaching > 4 mM. At Stations below  
381 the OMZ (Stations 9 and 10), no  $\text{H}_2\text{S}$  was detected within pore waters (Fig. 4).

382 Iron concentrations inside the benthic chambers reached maximum  
383 values > 300 nM. At Stations 4 and 6, located inside the OMZ, concentrations in the  
384 chambers increased in a linear way during the incubation. At stations above and  
385 below the OMZ, we did not observe a similar trend over time. For comparison with  
386 diffusive fluxes, we estimated benthic Fe fluxes from linear regressions of Fe  
387 concentrations versus time (Table 2). We also calculated the theoretical  
388 concentration gradients over time in the benthic chambers based on our diffusive flux  
389 estimates (Fig. 5). The incubation data were largely consistent in direction and slope  
390 with the diffusive fluxes. In particular, the projected and observed concentration  
391 gradients were in good agreement at stations inside the OMZ (Station 4 and 6),  
392 where the highest diffusive fluxes of -17.5 and -8.0  $\text{mmol m}^{-2} \text{y}^{-1}$  were observed. At  
393 these stations also the highest  $R^2$  for the linear regressions of the concentration  
394 change over the incubation time were calculated (Station 4:  $R^2 = 0.7$ , Station 6:  $R^2 =$

395 0.5) (Table S4). At stations below the OMZ, diffusive fluxes of  $< 1 \text{ mmol m}^{-2} \text{ y}^{-1}$  were  
396 too low to be detected over the incubation time of 32 hours.

397

### 398 **3.2.2 Cadmium**

399 In near-bottom waters Cd concentrations increased with distance from the  
400 coast, from 0.4 nM at the shallowest station at 75 m water depth (Station 1) to 1.1 nM  
401 below the OMZ at 750 m water depth (Station 9). Cadmium concentrations were  
402 constant at each station between 0.5 and 4 m above the seafloor (Fig. 3).

403 Cadmium concentrations in pore waters ranged between 0.1 – 2 nM (Fig. 6).  
404 Within the OMZ, bottom water concentrations were higher than concentrations in  
405 pore water at the sediment surface (0 - 1 cm), indicating a downward diffusive flux  
406 into the sediments. The benthic diffusive fluxes inside the OMZ were on the order of  
407  $0.6 - 0.8 \text{ } \mu\text{mol m}^{-2} \text{ y}^{-1}$  (Table 3). In contrast, at Stations 1 and 9 an upward-directed  
408 concentration gradient was observed, indicating a diffusive flux from the sediments  
409 into bottom waters. The upward diffusive flux was  $-1.9 \text{ } \mu\text{mol m}^{-2} \text{ y}^{-1}$  above the  
410 permanent OMZ and  $-0.2 \text{ } \mu\text{mol m}^{-2} \text{ y}^{-1}$  below the OMZ (Table 3). Pore water Cd  
411 concentrations at greater sediment depths were mostly higher than bottom water  
412 concentrations. In some cases (Stations 3 and 4), elevated pore water Cd  
413 concentrations (up to 2 nM) coincided with elevated  $\text{H}_2\text{S}$  concentrations (few hundred  
414  $\mu\text{M}$ ).

415 In the benthic chambers three different Cd trends were observed (Fig. 7).  
416 Above the permanent OMZ (Station 1), Cd concentrations in the chambers were low  
417 ( $< 0.2 \text{ nM}$ ) throughout the incubation period, indicating no Cd flux. At sites within the  
418 OMZ (Stations 4, 5 and 6), concentrations decreased from  $\sim 0.6 - 0.3 \text{ nM}$  over the  
419 course of the incubation. Below the OMZ (Stations 9 and 10), Cd concentrations in  
420 the chamber were high ( $\sim 1 \text{ nM}$ ) and remained constant or increased slightly during  
421 the incubation. At sites within the OMZ, Cd removal within the chamber was near-  
422 linear (Stations 4, 5 and 6:  $R^2 = \geq 0.9$ ) (Table S4), which translates to a removal flux  
423 of  $13 - 23 \text{ } \mu\text{mol m}^{-2} \text{ y}^{-1}$ . The Cd removal fluxes in benthic chambers were more than  
424 one order of magnitude higher than diffusive benthic fluxes ( $0.6 - 0.8 \text{ } \mu\text{mol m}^{-2} \text{ y}^{-1}$ )  
425 (Table 3).

426

427

## 428 **4. Discussion**

429

### 430 **4.1 Benthic iron cycling**

#### 431 **4.1.1 Comparison of diffusive and in-situ benthic chamber iron fluxes**

432 Concentrations of Fe in bottom waters from benthic chamber incubations are  
433 mostly higher than in ambient bottom waters because of Fe release from the  
434 sediment and an accumulation in the enclosed water volume inside the benthic  
435 chamber. In the absence of oxygen and, thus, bottom-dwelling macrofauna at  
436 stations within the OMZ, bioturbation and bioirrigation are unlikely to exert an  
437 important control on sedimentary Fe release. Consistent with this notion, the slope  
438 calculated from benthic diffusive fluxes is largely consistent with the concentration  
439 gradients observed within the benthic chambers (Fig. 5). Moreover, our fluxes from  
440 benthic chamber incubations and diffusive fluxes are generally of the same order of  
441 magnitude (Table 2). Therefore, diffusive transport of dissolved Fe from the sediment  
442 into the bottom water seems to be the main control on the concentration evolution  
443 observed within the benthic chamber.

444 Some of the concentration gradients in benthic chambers are non-linear,  
445 indicating that the Fe flux was not constant during the incubations. This is a common  
446 observation in Fe flux data from benthic chamber incubations and higher Fe fluxes  
447 generally have higher  $R^2$  values for the linear regressions (Friedrich et al., 2002;  
448 Turetta et al., 2005; Severmann et al., 2010; Lenstra et al., 2019). However, the non-  
449 linearity can be used to identify additional processes affecting Fe concentrations and  
450 fluxes within the benthic chamber, which may also affect fluxes under natural  
451 conditions. One possible process that can remove dissolved Fe(II) under anoxic  
452 conditions is Fe oxidation with  $\text{NO}_3^-$  as the terminal electron acceptor or oxidation  
453 with  $\text{NO}_2^-$  (Straub et al., 1996; Carlson et al., 2013; Klueglein and Kappler, 2013). The  
454 oxidation of reduced Fe in the absence of oxygen, either microbially mediated with  
455  $\text{NO}_3^-$  or abiotically with  $\text{NO}_2^-$ , has been hypothesized to be important in the water  
456 column of the Peruvian OMZ (Scholz et al., 2016; Heller et al., 2017). During our  
457 incubation at Station 4 (Fig. 8), we observed a decline in Fe concentrations during  
458 the first ten hours of the incubation time. Concurrently,  $\text{NO}_3^-$  concentrations were

459 decreasing, while  $\text{NO}_2^-$  accumulated, presumably due to progressive denitrification  
460 and release from the sediments. Once  $\text{NO}_3^-$  and  $\text{NO}_2^-$  were depleted, Fe  
461 concentrations started to rise again, resulting in the highest in-situ Fe flux observed  
462 throughout our sampling campaign (Table 2). The coincidence in timing of Fe  
463 accumulation and  $\text{NO}_2^-$  decrease suggest that depletion of Fe at the beginning of the  
464 incubation was most likely caused by Fe oxidation with  $\text{NO}_2^-$ . The incubation at  
465 Station 4 was the only one where  $\text{NO}_3^-$  and  $\text{NO}_2^-$  were substantially removed during  
466 the incubation. However, the high Fe flux cannot be interpreted as a natural flux  
467 estimate at steady state. In general, we argue that bottom water  $\text{NO}_2^-$  concentrations  
468 exert a first order control on the intensity of Fe efflux at the absence of oxygen and,  
469 therefore, need to be considered in the evaluation of sedimentary Fe mobility in  
470 anoxic-nitrogenous OMZs.

471 During the incubations at Stations 1, 9 and 10, Fe concentrations did not  
472 continuously increase but fluctuated between high and low values. This observation  
473 could be explained by a combination of bioirrigation and bioturbation at stations  
474 where oxygen was present (stations 9 and 10), as well as rapid Fe oxidation and  
475 precipitation processes. Under oxic conditions, bottom-dwelling macrofauna is likely  
476 to increase the transfer of dissolved Fe from the sediments into the bottom water  
477 (Elrod et al., 2004; Lenstra et al., 2019). During episodes of oxygenation a population  
478 of macrofauna that can enhance bioturbation and bioirrigation was observed on the  
479 Peruvian shelf (Gutiérrez et al., 2008). However, under oxic conditions, any Fe  
480 delivered to the chamber is prone to rapid oxidative removal. Moreover, ex-situ  
481 experiments have demonstrated a fast and efficient removal of up to 90% of  
482 dissolved Fe in incubated bottom waters due to particle resuspension (Homoky et al.,  
483 2012). Bioturbation and bioirrigation could also contribute to particle resuspension at  
484 oxic stations, thus leading to removal of dissolved Fe.

485 Furthermore, colloidal Fe could modify Fe concentrations within our samples  
486 and explain some of the fluctuations observed during the incubations. Colloids are  
487 quite reactive, they are much more soluble than larger particles and can be rapidly  
488 reduced and dissolved in anoxic environments, but they can also aggregate into  
489 larger particles (Raiswell and Canfield, 2012). The transfer of Fe between dissolved,  
490 colloidal and particulate pools is likely to affect the balance between Fe transport and  
491 re-precipitation and -deposition to some extent. However, since did not differentiate



492 between colloidal and truly dissolved fractions during our sampling, we cannot  
493 discuss this aspect further based on our data.

494 Oxidation processes and interactions with particles can efficiently remove Fe  
495 shortly after its transfer to bottom waters and this process is likely to be most intense  
496 close to the seafloor where the highest particle concentrations prevail. We argue that  
497 the same processes are reflected by declining Fe concentrations away from the  
498 seafloor in some of the bottom water profiles (at Stations 3 and 4) (Fig. 3).

499

#### 500 **4.1.2 Removal rates of dissolved iron in the near-bottom water column**

501 We observed declining Fe concentrations in the first 4 m away from the  
502 seafloor at Stations 3 and 4, which hints at removal of dissolved Fe in the near  
503 bottom waters after its release from the sediments. To differentiate between dilution  
504 with ambient bottom water (by currents) from Fe removal from the dissolved phase,  
505 Fe concentrations were normalized by Si(OH)<sub>4</sub> measured in the same samples (Fig.  
506 3). Due to opal dissolution within Peru margin sediments, Si(OH)<sub>4</sub> is released into  
507 bottom waters (Ehlert et al., 2016). In contrast to Fe, we assume that Si(OH)<sub>4</sub>  
508 behaves conservatively and precipitation reactions within the bottom waters are of  
509 subordinate importance. The decreasing Fe to Si(OH)<sub>4</sub> ratios at Station 3 and 4 with  
510 distance from the seafloor indicate that there is Fe removal within the near-bottom  
511 water column that must be related to precipitation processes or scavenging.

512 We further constrained rates of dissolved Fe removal at stations with a  
513 discernable Fe to Si(OH)<sub>4</sub> gradient within the first 4 m distance from the seafloor. To  
514 this end, we first determined an eddy diffusion coefficient ( $K_y$ ) using Si(OH)<sub>4</sub> fluxes  
515 from benthic chamber incubations ( $F_{Si}$ ) (see chapter 2.3 for methodology) and the  
516 known concentration gradient of dissolved Si(OH)<sub>4</sub> within the bottom water ( $d_{Si}/d_x$ ),  
517 where  $x$  is the height above the seafloor. At the seafloor, the flux of Si(OH)<sub>4</sub> from the  
518 sediment is equal to the flux in the water column.

$$519 \quad F_{Si} = -K_y(d_{Si}/d_x) \quad (4)$$

520 This equation can be solved for the eddy diffusion coefficient.

521 Dissolved Fe in the bottom water (DFe) can be described by the solving the  
522 diffusion-reaction equation for DFe (ignoring advection and assuming a steady-state  
523 first-order consumption of dissolved Fe):

$$524 \quad DFe = C_{BW} * \exp.(-\sqrt{k_{Feox}}/\sqrt{K_y}) \quad (5)$$

525 The equation can be fitted to the measured DFe concentrations in the bottom water  
526 by adjusting the Fe concentration directly above the seafloor ( $C_{BW}$ ) and the Fe  
527 oxidation constant ( $k_{Feox}$ ). From the fitted first-order rate constant  $k_{Feox}$ , the half-life for  
528 dissolved Fe in bottom waters can be calculated.

529 The half-lives of dissolved Fe in the first 4 m away from the seafloor are 2.5  
530 min and 0.3 min at Stations 3 and 4, respectively (Table 4). Another study reported a  
531 dissolved Fe half-life of 17 hours under nitrogenous conditions in the first 10 – 20 m  
532 above the seafloor in the Peruvian OMZ (Scholz et al., 2016). Our calculations  
533 suggest that Fe removal in near-bottom waters is much faster. The approach  
534 assumes that  $Si(OH)_4$  is transported vertically by eddy diffusion and eddy diffusion  
535 and oxidation control the half-life of Fe in the first 4 m above the seafloor. It is  
536 possible that our assumption of solute transport by eddy diffusion is not correct.  
537 Alternatively, decreasing Fe and  $Si(OH)_4$  concentration above the seafloor could be  
538 due to super-imposed water layers with different Fe and  $Si(OH)_4$  concentrations but  
539 little vertical exchange. In this case our calculated half-life would be an  
540 underestimation.

541 As mentioned above (chapter 4.1.1), in the absence of oxygen, removal  
542 processes of dissolved Fe could be related to oxidation of dissolved Fe with  $NO_2^-$  or  
543 to interactions with suspended particles, which are likely to be most abundant directly  
544 above the seafloor. Further research on dissolved-particulate interactions, including  
545 the role of colloidal Fe, in bottom waters is needed to better constrain how  
546 sedimentary Fe fluxes are modified in the near-bottom water column.

547

#### 548 **4.1.3 Controls on the temporal variability of benthic iron fluxes**

549 The Peruvian OMZ is known to experience high-amplitude fluctuations in  
550 upwelling intensity as well as variability in bottom water oxygen,  $NO_3^-$ ,  $NO_2^-$  and  $H_2S$   
551 concentrations (Pennington et al., 2006; Gutiérrez et al., 2008; Graco et al., 2017;

552 Ohde, 2018). To get an insight into how different biogeochemical conditions control  
553 benthic diffusive Fe(II) fluxes, we compared the fluxes from our recent cruise with  
554 fluxes from our earlier cruise M92 (Fig. 9). Cruise M92 took place in austral autumn  
555 2013 following the main upwelling season and during a period of intense primary  
556 productivity. Due to reduced upwelling and stable density stratification, the water  
557 column on the shallow shelf was not only depleted in oxygen but also in  $\text{NO}_3^-$  and  
558  $\text{NO}_2^-$  during cruise M92 (Sommer et al., 2016). Under such conditions,  
559 chemolithoautotrophic  $\text{H}_2\text{S}$  oxidation with  $\text{NO}_3^-$  or  $\text{NO}_2^-$  was impeded so that pore  
560 water  $\text{H}_2\text{S}$  could be released from the sediment into the water column. As a result,  
561 the water column during M92 was sulfidic between around 50 – 150 m water depth  
562 with the highest  $\text{H}_2\text{S}$  concentration of 13  $\mu\text{M}$  observed at 50 m depth (Fig. 2). While  
563 the biogeochemical conditions on the shallow shelf were fundamentally different to  
564 those during M136 and M137, below 150 m water depth the conditions were largely  
565 comparable (oxygen-depleted,  $\text{NO}_3^-$ : 20 – 30  $\mu\text{M}$ ,  $\text{NO}_2^-$  up to 9  $\mu\text{M}$  between 150 –  
566 300 m). At the stations with similar biogeochemical water column conditions, the  
567 Fe(II) fluxes during both sampling campaigns were remarkably similar (Fig. 9).  
568 However, similar to the temporal variability of Fe concentrations in bottom waters at  
569 Station 1 (Fig. 3), we observed a pronounced difference in the diffusive flux  
570 magnitude on the shallow shelf where the biogeochemical conditions differed  
571 between both cruises. The highest diffusive flux during M92 in 2013 of  $-22.7 \text{ mmol m}^{-2} \text{ y}^{-1}$   
572 was measured at Station 1. By contrast, during M136/137 in 2017 we  
573 determined a much lower flux of  $-2.6 \text{ mmol m}^{-2} \text{ y}^{-1}$  at this station. During M136 and  
574 M137 the highest flux of  $-17.5 \text{ mmol m}^{-2} \text{ y}^{-1}$  was measured at Station 4 at 145 m  
575 water depth.

576 Diffusive fluxes are a function of the concentration gradient between pore  
577 water and bottom water (Eq. (1)). As dissolved Fe concentrations in bottom waters  
578 are generally much lower (nM) compared to those observed in pore waters ( $\mu\text{M}$ ), the  
579 flux magnitude is chiefly determined by differences in pore water Fe concentrations.  
580 During M92, pore waters at the sediment surface were characterized by high  
581 dissolved Fe concentrations (4.8  $\mu\text{M}$  in the upper pore water sample), which resulted  
582 in a steep gradient and a comparably high Fe flux. Under the slightly sulfidic  
583 conditions that prevailed in the water column during M92, oxidative removal of  
584 dissolved Fe(II) with  $\text{NO}_3^-$  or  $\text{NO}_2^-$  was impeded (Scholz et al., 2016) and dissolved  
585 Fe(II) could be stabilized as aqueous iron sulfide (Schlosser et al., 2018). Therefore,

586 the bottom water was characterized by high dissolved Fe concentrations (up to 0.7  
587  $\mu\text{M}$  in the supernatant bottom water of MUCs).

588 Despite oxic conditions in the water column during M136 and M137, we  
589 observed much higher  $\text{H}_2\text{S}$  concentrations in surface sediments at Station 1  
590 compared to M92 (4100  $\mu\text{M}$  during M136 and M137 versus 1800  $\mu\text{M}$  during M92  
591 within the first 8 cm of the core) (Fig. 4). Because of higher  $\text{H}_2\text{S}$  concentrations, Fe  
592 concentrations were controlled by the solubility of Fe monosulfide minerals ( $\text{FeS}$ ). It  
593 may seem counterintuitive that the surface sediment was highly sulfidic, while the  
594 overlying water column was oxygenated. In order to explain this observation, we  
595 need to consider the role of mats of filamentous sulfur oxidizing bacteria in controlling  
596  $\text{H}_2\text{S}$  concentrations in surface sediments. (Gutiérrez et al., 2008; Noffke et al., 2012;  
597 Yücel et al., 2017). During M92 these mats were generally abundant on the shelf and  
598 upper slope (Sommer et al., 2016), thus limiting the extent of  $\text{H}_2\text{S}$  accumulation  
599 within surface sediments. Previous studies demonstrated that mats of sulfur oxidizing  
600 bacteria can disappear during periods of oxygenation (Gutiérrez et al., 2008).  
601 Consistent with this previous finding, visual inspection of the seafloor using the video-  
602 guided MUC revealed that the abundance of bacterial mats on the seafloor seemed  
603 greatly reduced, which is most probably related to oxic bottom water conditions on  
604 the shallow shelf during the coastal El Niño event. As these microaerophilic  
605 organisms tend to avoid high oxygen concentrations they probably started to die off  
606 or withdraw into the sediment once oxygen levels raised. We suggest that the  
607 disappearance of sulfide-oxidizing bacteria under oxic conditions created a situation  
608 where  $\text{H}_2\text{S}$  accumulation in the surface sediment and  $\text{FeS}$  precipitation limited the  
609 extent of Fe release into the bottom water.

610

## 611 **4.2 Benthic cadmium cycling**

### 612 **4.2.1 Comparison of diffusive and in-situ benthic chamber cadmium fluxes**

613 At stations above and below the permanent OMZ (Stations 1, 9 and 10),  
614 diffusive Cd fluxes and fluxes in benthic chambers were largely consistent (Table 3).  
615 In contrast, the fluxes determined with benthic chambers at stations within the OMZ  
616 (Station 4, 5 and 6) were 25 to 40 times higher than the diffusive flux (Table 3). This  
617 discrepancy demonstrates that diffusion cannot be the dominant process leading to

618 the continuous decrease of dissolved Cd during benthic chamber incubations.  
619 Alternatively, Cd could be precipitated within the benthic chamber and removed  
620 through downward sinking of Cd-rich particles. Cadmium sulfide (greenockite) has a  
621 relatively low solubility compared to sulfide minerals of other TMs ( $\text{CdS} \ll \text{FeS}$ ). It is  
622 generally agreed that CdS precipitation can take place at trace amounts of  $\text{H}_2\text{S}$  ( $\text{H}_2\text{S}$   
623  $< 1 \mu\text{M}$ , i.e., below the detection limit of the method applied in this study) (Davies-  
624 Colley et al., 1985; Rosenthal et al., 1995). Previous studies using in-situ benthic flux  
625 chambers have concluded that production of  $\text{H}_2\text{S}$  in the sediment or the accumulation  
626 of  $\text{H}_2\text{S}$  in benthic chambers during incubations can switch the direction of the Cd flux  
627 or intensify Cd removal through CdS precipitation (Westerlund et al., 1986; Colbert et  
628 al., 2001). Precipitation of CdS during the incubation is, therefore, a viable  
629 explanation for the discrepancy between diffusive Cd flux and Cd fluxes in benthic  
630 chambers observed in our study. Furthermore, the three different trends of Cd  
631 concentrations observed in benthic chamber incubations can be related to  $\text{H}_2\text{S}$   
632 concentrations in the surface sediment below the benthic chambers (Table 3). At  
633 stations within the OMZ (Stations 4,5 and 6), pore water  $\text{H}_2\text{S}$  concentrations in  
634 surface sediments were moderate (few  $\mu\text{M}$ ). It is likely that there was a continuous  
635 leakage of trace amounts of  $\text{H}_2\text{S}$  from the pore water into the bottom waters during  
636 the incubation, thus leading to CdS precipitation and declining Cd concentrations. On  
637 the shallowest shelf station (Station 1), where pore water  $\text{H}_2\text{S}$  concentrations in the  
638 surface sediment were high (hundreds of  $\mu\text{M}$ ), a potentially large amount could have  
639 been released at the beginning of the incubation, thus explaining pronounced Cd  
640 depletion in the chamber compared to the surrounding bottom water (0.1 nM within  
641 the chamber compared to 0.4 nM outside the chamber). Below the OMZ (Stations 9  
642 and 10), where there was no  $\text{H}_2\text{S}$  present in surface sediments, there was no Cd  
643 depletion in the chamber during the incubation and, consistent with previous studies  
644 in oxic settings (Westerlund et al., 1986; Ciceri et al., 1992; Zago et al., 2000; Turetta  
645 et al., 2005), both diffusive and benthic chamber flux data were indicative of an  
646 upward-directed flux out of the sediment. Due to the absence of  $\text{H}_2\text{S}$ , dissolved Cd  
647 released from biogenic particles in the surface sediment could accumulate in the pore  
648 water thus driving a diffusive flux out of the sediment.

649

#### 650 **4.2.2 Quantification of the sedimentary cadmium sink**

651 Consistent with our Cd flux data there is general consent that OMZs are a sink  
652 for Cd. Several water column studies have observed Cd depletion in water masses  
653 within the Peruvian and other OMZs, which was mostly attributed to Cd removal via  
654 CdS precipitation in sulfidic micro-niches within particles in the water column  
655 (Janssen et al., 2014; Conway and John, 2015b). Sedimentary studies showed that  
656 Cd is highly enriched in OMZ sediments, which has mostly been attributed to the  
657 delivery of Cd with organic material and subsequent fixation as CdS within sulfidic  
658 sediments (Ragueneau et al., 2000; Böning et al., 2004; Borchers et al., 2005;  
659 Muñoz et al., 2012; Little et al., 2015). Based on our data, we can quantify the  
660 delivery of Cd to the sediments via three different pathways: (1) diffusion across the  
661 sediment-water interface and CdS precipitation within the sediment; (2) Cd  
662 incorporation by phytoplankton and delivery to the sediment with organic matter; (3)  
663 CdS precipitation in the water column and particulate delivery to the sediment (Table  
664 3).

665 The enrichment of Cd in the sediment relative to the lithogenic background  
666 (expressed as excess Cd concentration;  $Cd_{xs}$ ) was calculated using the following  
667 equation (Brumsack, 2006):

$$668 \quad Cd_{xs} = Cd_{sample} - Al_{sample} * (Cd/Al)_{crust} \quad (6)$$

669 The Cd/Al ratio of the upper continental crust ( $1.22 \cdot 10^{-6}$ ) was used as lithogenic  
670 background reference (Taylor and McLennan, 2009). To calculate the flux of Cd to  
671 the sediment,  $Cd_{xs}$  was multiplied with the mass accumulation rate (MAR) from  
672 published data for each individual site (Dale et al., 2015b). To approximate the  
673 amount of Cd delivered to the sediment with organic material, the average  
674 concentration ratio of Cd to C in phytoplankton (Moore et al., 2013) was multiplied by  
675 published particulate organic carbon rain rates (maximum estimate) or burial rates  
676 (minimum estimate) for each individual site (Dale et al., 2015b). The Cd delivery via  
677 precipitation in the water column was determined as the remainder of  $Cd_{xs} * MAR$   
678 after subtraction of the two other sources (i.e., diffusive flux and minimum/maximum  
679 delivery by organic material).

680 Sediments at all stations on the Peruvian shelf and slope are enriched in Cd  
681 relative to the lithogenic background. The accumulation rate of Cd decreases with  
682 distance from the coast from  $250 \mu\text{mol m}^{-2} \text{y}^{-1}$  at Station 1 to  $4 \mu\text{mol m}^{-2} \text{y}^{-1}$  at Station

683 9 (Table 3). These fluxes generally exceed the amount of Cd delivered to the  
684 sediments via diffusion and associated with organic material. Together these  
685 mechanisms of Cd delivery can only account for ~ 20 % of the Cd enrichment at  
686 stations above and inside the permanent OMZ, with the delivery with organic material  
687 being of greater importance. The remaining Cd enrichment in the sediment (~ 80 %),  
688 after subtraction of diffusive and minimum/maximum organic Cd sources, must be  
689 related to CdS precipitation in the water column and delivery of Cd-rich particles to  
690 the sediment. This removal process can be a combination of CdS precipitation in  
691 sulfidic micro-niches around sinking particles (Janssen et al., 2014; Bianchi et al.,  
692 2018), CdS precipitation in sulfide plumes (Xie et al., 2019) when sedimentary H<sub>2</sub>S  
693 can spread throughout the water column (Schunck et al., 2013; Ohde, 2018), and  
694 precipitation of CdS in the near-bottom water (this study). Our estimated CdS  
695 precipitation in the water column within the OMZ agrees with the Cd fluxes  
696 determined from benthic chamber incubations, where dissolved Cd removal takes  
697 place in the 20 – 30 cm of overlying water above the seafloor. These Cd removal  
698 fluxes from benthic chambers alone are sufficient to account for 41 % – 68 % of the  
699 estimated particulate Cd removal from the water column and 38 % – 60 % of total Cd  
700 enrichment in the sediment within the OMZ (Table 3). Considering that Cd  
701 precipitation in near-bottom water is unlikely to be restricted to the 20 – 30 cm above  
702 the seafloor, covered by our benthic chambers, the removal flux associated with this  
703 process is likely to be even higher. At Station 1, where the surface sediment below  
704 the benthic chamber was highly sulfidic, the particulate Cd removal calculated from  
705 the concentration difference between the bottom water (0.5 m) and the first sample  
706 from the benthic chamber incubation (taken after 0.25 h) was high enough to explain  
707 the total Cd enrichment in the sediment.

708 Below the OMZ, at Station 9, where the smallest Cd enrichment was observed, the  
709 relative contribution of Cd delivery with organic material increases. About half of the  
710 Cd enrichment can be attributed to organic material at this station.

711 Once Cd is delivered to the sediment, it can either stay fixed in the solid phase  
712 or be released to the pore waters. Cadmium concentrations in pore waters of  
713 subsurface sediments (> 10 cm sediment depth) were mostly higher than bottom  
714 water concentrations (Fig. 6), indicating a transfer of Cd from the solid phase into  
715 pore waters during early diagenesis. Cadmium sulfides are considered highly

716 insoluble and stable within sediments (Elderfield et al., 1981), even upon re-  
717 oxygenation (Rosenthal et al., 1995). Therefore, Cd release through re-dissolution of  
718 CdS is ruled out as a potential source of dissolved Cd. Alternatively, Cd liberation  
719 upon remineralization of organic material could explain elevated Cd concentrations in  
720 the pore water. Elevated Cd concentrations in sulfidic pore waters have been  
721 observed in previous studies and attributed to Cd stabilization through formation of  
722 organic and inorganic complexes (Gobeil et al., 1987; Sundby et al., 2004).  
723 Experimental data gave evidence for the presence of dissolved Cd bisulfide and  
724 polysulfide complexes in pore waters. An increase of electrochemically active Cd  
725 after UV irradiation, was explained by the destruction of electrochemically inactive  
726 bisulfide and polysulfide complexes (Gobeil et al., 1987). At very high H<sub>2</sub>S  
727 concentrations ( $> 10^{-3}$  M) the solubility of Cd may increase due to an increase in  
728 these bisulfide and polysulfide complexes. Under such highly sulfidic conditions, Cd  
729 solubility may even exceed the solubility in oxygenated waters and highly sulfidic  
730 sediment can eventually lead to a diffusive source of Cd to the bottom water (Davies-  
731 Colley et al., 1985). Such a scenario may explain the negative (i.e., upward-directed)  
732 diffusive Cd flux at Station 1, where the pore waters of surface sediments are highly  
733 sulfidic.

734

735

## 736 **5. Conclusions and implications for trace metal sources and sinks in the future** 737 **ocean**

738 Consistent with earlier work, our results demonstrate that that OMZ sediments  
739 are a source for Fe and a sink for Cd. Moreover, based on our findings,  
740 biogeochemical conditions and processes that control the benthic fluxes of these TM  
741 across the Peruvian OMZ can be further constrained.

742 Within the OMZ, where bottom dwelling macrofauna is absent, diffusion is the  
743 main process that transports Fe from the sediment pore water into the bottom water.  
744 The accumulation of high levels of H<sub>2</sub>S in pore waters, modulated by the abundance  
745 of sulfur oxidizing bacteria, can reduce diffusive Fe release through sulfide  
746 precipitation within pore waters. In anoxic bottom waters Fe can be rapidly removed,  
747 likely via oxidation with NO<sub>2</sub><sup>-</sup> and/or interaction with particles. Benthic Cd fluxes are



748 directed from the bottom water into the sediment within the OMZ. Diffusive fluxes and  
749 delivery of Cd via organic material cannot account for the sedimentary Cd  
750 enrichment. Instead CdS precipitation in near-bottom waters could be the most  
751 important pathway that delivers Cd to the sediments.

752 According to our results, H<sub>2</sub>S concentrations in surface sediments exert a first  
753 order control on the magnitude and direction of Fe and Cd fluxes across the  
754 sediment-water interface. With generally decreasing oxygen concentrations in the  
755 ocean and an expansion of OMZs (Stramma et al., 2008; Schmidtko et al., 2017),  
756 sulfidic surface sediments will likely also expand. With regard to the solubility of their  
757 sulfide minerals, Fe and Cd represent two opposite end members. The solubility of  
758 sulfide minerals of other important nutrient-type TMs, such as Ni and Zn, is  
759 intermediate between those of Fe and Cd (Fe > Ni > Zn > Cd). An expansion of  
760 sulfidic surface sediments is thus likely to affect sedimentary TM fluxes in a differing  
761 manner. This notion is illustrated in Fig. 10, showing saturation indices calculated  
762 based on the range of TM concentrations observed in the ocean and typical H<sub>2</sub>S  
763 concentrations observed in anoxic marine environments (nM – μM concentrations  
764 represent sulfidic events in the water column; μM – mM concentrations are typical for  
765 pore waters). Cadmium sulfide minerals become oversaturated at nM to μM H<sub>2</sub>S  
766 concentrations, which explains why Cd removal can take place in the bottom water in  
767 OMZs. By contrast, FeS is highly undersaturated under the typical biogeochemical  
768 conditions in the water column. Therefore, FeS precipitation is unlikely to take place  
769 in the water column, even under somewhat more reducing conditions. Other sulfide-  
770 forming TMs have an intermediate sulfide solubility (e.g. Zn, Ni), which could imply  
771 that the direction and magnitude of their sedimentary fluxes is susceptible to  
772 expanding ocean anoxia. The differing response of TMs to an expansion of sulfidic  
773 conditions may cause a change in the TM stoichiometry of upwelling water masses  
774 with potential consequences for TM-dependent marine ecosystems in surface waters.

775

776

#### 777 **Data availability**

778 The data will be made available at Pangaea upon publication of the article.

779

780

781 **Author contribution**

782 AP and FS conceived the study. AP, FS, AD, SS conducted the sampling at sea. AP  
783 analyzed the trace metal concentrations. AP and FS prepared the manuscript with  
784 contributions from all co-authors.

785

786

787 **Competing Interests**

788 The authors declare that they have no conflict of interest.

789

790

791 **Acknowledgements**

792 We are grateful for the support of the crew of RV Meteor during the fieldwork. For  
793 their technical and analytical assistance we thank A. Beck, A. Bleyer, B. Domeyer, D.  
794 Jasinski, A. Petersen, T. Steffens, R. Surberg and M. Türk. This study was supported  
795 by the German Research Foundation through the Emmy Noether  
796 Nachwuchsforschergruppe ICONOX (Iron Cycling in Continental Margin Sediments  
797 and the Nutrient and Oxygen Balance of the Ocean) and Sonderforschungsbereich  
798 754 (Climate-Biogeochemistry Interactions in the Tropical Ocean). We also would like  
799 to thank Edouard Metzger and Michael Staubwasser for their constructive reviews, as  
800 well as S. Wajih A. Naqvi for the editorial handling.

801 **References**

802

803 Audry, S., Blanc, G., Schäfer, J., Chaillou, G. and Robert, S.: Early diagenesis of  
804 trace metals (Cd, Cu, Co, Ni, U, Mo, and V) in the freshwater reaches of a macrotidal  
805 estuary, *Geochim. Cosmochim. Acta*, 70(9), 2264–2282,  
806 doi:10.1016/j.gca.2006.02.001, 2006.

807 Ball, J. W. and Nordstrom, D. K.: WATEQ4F -- User's manual with revised  
808 thermodynamic data base and test cases for calculating speciation of major, trace  
809 and redox elements in natural waters, US Geol. Surv., (Open-File Rep.), 91–183,  
810 doi:10.3133/ofr90129, 1991.

811 Bianchi, D., Weber, T. S., Kiko, R. and Deutsch, C.: Global niche of marine anaerobic  
812 metabolisms expanded by particle microenvironments, *Nat. Geosci.*, 11(April), 1–6,  
813 doi:10.1038/s41561-018-0081-0, 2018.

814 Biller, D. V. and Bruland, K. W.: Sources and distributions of Mn, Fe, Co, Ni, Cu, Zn,  
815 and Cd relative to macronutrients along the central California coast during the spring  
816 and summer upwelling season, *Mar. Chem.*, 155, 50–70,  
817 doi:10.1016/j.marchem.2013.06.003, 2013.

818 Böning, P., Brumsack, H. J., Böttcher, M. E., Schnetger, B., Kriete, C., Kallmeyer, J.  
819 and Borchers, S. L.: Geochemistry of Peruvian near-surface sediments, *Geochim.  
820 Cosmochim. Acta*, 68(21), 4429–4451, doi:10.1016/j.gca.2004.04.027, 2004.

821 Bopp, L., Le Quéré, C., Heimann, M., Manning, A. C. and Monfray, P.: Climate-  
822 induced oceanic oxygen fluxes: Implications for the contemporary carbon budget,  
823 *Global Biogeochem. Cycles*, 16(2), 6-1-6–13, doi:10.1029/2001GB001445, 2002.

824 Borchers, S. L., Schnetger, B., Böning, P. and Brumsack, H.-J.: Geochemical  
825 signatures of the Namibian diatom belt: Perennial upwelling and intermittent anoxia,  
826 *Geochemistry, Geophys. Geosystems*, 6(6), doi:10.1029/2004GC000886, 2005.

827 Boudreau, B. P.: *Diagenetic Models and Their Implementation*, Springer., 1997.

828 Boyd, P. W. and Ellwood, M. J.: The biogeochemical cycle of iron in the ocean, *Nat.  
829 Geosci.*, 3(10), 675–682, doi:10.1038/ngeo964, 2010.

830 Bruland, K. W. and Lohan, M. C.: Controls of Trace Metals in Seawater, in *Treatise*

831 on Geochemistry, pp. 23–47, Elsevier., 2003.

832 Brumsack, H. J.: The trace metal content of recent organic carbon-rich sediments:  
833 Implications for Cretaceous black shale formation, *Palaeogeogr. Palaeoclimatol.*  
834 *Palaeoecol.*, 232(2–4), 344–361, doi:10.1016/j.palaeo.2005.05.011, 2006.

835 Canfield, D. E.: Reactive iron in marine sediments, *Geochim. Cosmochim. Acta*,  
836 53(3), 619–632, doi:10.1016/0016-7037(89)90005-7, 1989.

837 Carlson, H. K., Clark, I. C., Blazewicz, S. J., Iavarone, A. T. and Coates, J. D.: Fe(II)  
838 Oxidation Is an Innate Capability of Nitrate-Reducing Bacteria That Involves Abiotic  
839 and Biotic Reactions, *J. Bacteriol.*, 195(14), 3260–3268, doi:10.1128/JB.00058-13,  
840 2013.

841 Ciceri, G., Maran, C., Martinotti, W. and Queirazza, G.: Geochemical cycling of heavy  
842 metals in a marine coastal area: benthic flux determination from pore water profiles  
843 and in situ measurements using benthic chambers, *Hydrobiologia*, 235–236(1), 501–  
844 517, doi:10.1007/BF00026238, 1992.

845 Colbert, D., Coale, K. ., Berelson, W. . and Johnson, K. .: Cadmium Flux in Los  
846 Angeles/Long Beach Harbours and at Sites along the California Continental Margin,  
847 *Estuar. Coast. Shelf Sci.*, 53(2), 169–180, doi:10.1006/ecss.2001.0802, 2001.

848 Collier, R. and Edmond, J.: The trace element geochemistry of marine biogenic  
849 particulate matter, *Prog. Oceanogr.*, 13(2), 113–199, doi:10.1016/0079-  
850 6611(84)90008-9, 1984.

851 Conway, T. M. and John, S. G.: Quantification of dissolved iron sources to the North  
852 Atlantic Ocean, *Nature*, 511(7508), 212–215, doi:10.1038/nature13482, 2014.

853 Conway, T. M. and John, S. G.: Biogeochemical cycling of cadmium isotopes along a  
854 high-resolution section through the North Atlantic Ocean, *Geochim. Cosmochim.*  
855 *Acta*, 148, 269–283, doi:10.1016/j.gca.2014.09.032, 2015a.

856 Conway, T. M. and John, S. G.: The cycling of iron, zinc and cadmium in the North  
857 East Pacific Ocean - Insights from stable isotopes, *Geochim. Cosmochim. Acta*, 164,  
858 262–283, doi:10.1016/j.gca.2015.05.023, 2015b.

859 Dale, A. W., Nickelsen, L., Scholz, F., Hensen, C., Oeschlies, A. and Wallmann, K.: A  
860 revised global estimate of dissolved iron fluxes from marine sediments, *Global*

861 Biogeochem. Cycles, 29(5), 691–707, doi:10.1002/2014GB005017, 2015a.

862 Dale, A. W., Sommer, S., Lomnitz, U., Montes, I., Treude, T., Liebetrau, V., Gier, J.,  
863 Hensen, C., Dengler, M., Stolpovsky, K., Bryant, L. D. and Wallmann, K.: Organic  
864 carbon production, mineralisation and preservation on the Peruvian margin,  
865 Biogeosciences, 12(5), 1537–1559, doi:10.5194/bg-12-1537-2015, 2015b.

866 Dalsgaard, T., Thamdrup, B., Farías, L. and Revsbech, N. P.: Anammox and  
867 denitrification in the oxygen minimum zone of the eastern South Pacific, Limnol.  
868 Oceanogr., 57(5), 1331–1346, doi:10.4319/lo.2012.57.5.1331, 2012.

869 Davies-Colley, R. J., Nelson, P. O. and Williamson, K. J.: Sulfide control of cadmium  
870 and copper concentrations in anaerobic estuarine sediments, Mar. Chem., 16(2),  
871 173–186, doi:10.1016/0304-4203(85)90021-0, 1985.

872 Echevin, V., Colas, F., Espinoza-Morriberon, D., Vasquez, L., Anculle, T. and  
873 Gutierrez, D.: Forcings and Evolution of the 2017 Coastal El Niño Off Northern Peru  
874 and Ecuador, Front. Mar. Sci., 5(October), 1–16, doi:10.3389/fmars.2018.00367,  
875 2018.

876 Ehlert, C., Doering, K., Wallmann, K., Scholz, F., Sommer, S., Grasse, P., Geilert, S.  
877 and Frank, M.: Stable silicon isotope signatures of marine pore waters – Biogenic  
878 opal dissolution versus authigenic clay mineral formation, Geochim. Cosmochim.  
879 Acta, 191, 102–117, doi:10.1016/j.gca.2016.07.022, 2016.

880 Elderfield, H., McCaffrey, R. J., Luedtke, N., Bender, M. and Truesdale, V. W.:  
881 Chemical diagenesis in Narragansett Bay sediments, Am. J. Sci., 281(8), 1021–1055,  
882 doi:10.2475/ajs.281.8.1021, 1981.

883 Elrod, V. A., Berelson, W. M., Coale, K. H. and Johnson, K. S.: The flux of iron from  
884 continental shelf sediments: A missing source for global budgets, Geophys. Res.  
885 Lett., 31(12), n/a-n/a, doi:10.1029/2004GL020216, 2004.

886 Fitzsimmons, J. N., Conway, T. M., Lee, J.-M., Kayser, R., Thyng, K. M., John, S. G.  
887 and Boyle, E. A.: Dissolved iron and iron isotopes in the southeastern Pacific Ocean,  
888 Global Biogeochem. Cycles, 30(10), 1372–1395, doi:10.1002/2015GB005357, 2016.

889 Friedrich, J., Dinkel, C., Friedl, G., Pimenov, N., Wijsman, J., Gomoiu, M.-T.,  
890 Cociasu, A., Popa, L. and Wehrli, B.: Benthic Nutrient Cycling and Diagenetic  
891 Pathways in the North-western Black Sea, Estuar. Coast. Shelf Sci., 54(3), 369–383,

892 doi:10.1006/ecss.2000.0653, 2002.

893 Garreaud, R. D.: A plausible atmospheric trigger for the 2017 coastal El Niño, *Int. J.*  
894 *Climatol.*, 38(January 2017), e1296–e1302, doi:10.1002/joc.5426, 2018.

895 Gendron, A., Silverberg, N., Sundby, B. and Lebel, J.: Early diagenesis of cadmium  
896 and cobalt in sediments of the Laurentian Trough, *Geochim. Cosmochim. Acta*,  
897 50(5), 741–747, doi:10.1016/j.ijmachtools.2007.10.013, 1986.

898 Gerringa, L. J. A.: Aerobic degradation of organic matter and the mobility of Cu, Cd,  
899 Ni, Pb, Zn, Fe and Mn in marine sediment slurries, *Mar. Chem.*, 29(C), 355–374,  
900 doi:10.1016/0304-4203(90)90023-6, 1990.

901 Gobeil, C., Silverberg, N., Sundby, B. and Cossa, D.: Cadmium diagenesis in  
902 Laurentian Trough sediments, *Geochim. Cosmochim. Acta*, 51(3), 589–596,  
903 doi:10.1016/0016-7037(87)90071-8, 1987.

904 Graco, M. I., Purca, S., Dewitte, B., Castro, C. G., Morón, O., Ledesma, J., Flores, G.  
905 and Gutiérrez, D.: The OMZ and nutrient features as a signature of interannual and  
906 low-frequency variability in the Peruvian upwelling system, *Biogeosciences*, 14(20),  
907 4601–4617, doi:10.5194/bg-14-4601-2017, 2017.

908 Grasshoff, M., Erhardt, M. and Kremling, K.: *Methods of seawater analysis.*, Wiley-  
909 VCH, Weinheim, doi:10.1002/ange.19770890738, 1999.

910 Gutiérrez, D., Enríquez, E., Purca, S., Quipúzcoa, L., Marquina, R., Flores, G. and  
911 Graco, M.: Oxygenation episodes on the continental shelf of central Peru: Remote  
912 forcing and benthic ecosystem response, *Prog. Oceanogr.*, 79(2–4), 177–189,  
913 doi:10.1016/j.pocean.2008.10.025, 2008.

914 Hawco, N. J., Ohnemus, D. C., Resing, J. A., Twining, B. S. and Saito, M. A.: A  
915 dissolved cobalt plume in the oxygen minimum zone of the eastern tropical South  
916 Pacific, *Biogeosciences*, 13(20), 5697–5717, doi:10.5194/bg-13-5697-2016, 2016.

917 Heller, M. I., Lam, P. J., Moffett, J. W., Till, C. P., Lee, J. M., Toner, B. M. and  
918 Marcus, M. A.: Accumulation of Fe oxyhydroxides in the Peruvian oxygen deficient  
919 zone implies non-oxygen dependent Fe oxidation, *Geochim. Cosmochim. Acta*, 211,  
920 174–193, doi:10.1016/j.gca.2017.05.019, 2017.

921 Helm, K. P., Bindoff, N. L. and Church, J. A.: Observed decreases in oxygen content

922 of the global ocean, *Geophys. Res. Lett.*, 38(23), 1–6, doi:10.1029/2011GL049513,  
923 2011.

924 Homoky, W. B., Severmann, S., McManus, J., Berelson, W. M., Riedel, T. E.,  
925 Statham, P. J. and Mills, R. A.: Dissolved oxygen and suspended particles regulate  
926 the benthic flux of iron from continental margins, *Mar. Chem.*, 134–135, 59–70,  
927 doi:10.1016/j.marchem.2012.03.003, 2012.

928 Hydes, D., Aoyama, M., Aminot, A., Bakker, K., Becker, S., Coverly, S., Daniel, A.,  
929 Dickson, A. G., Grosso, O., Kerouel, R., van Ooijen, J., Sato, K., Tanhua, T.,  
930 Woodward, E. M. S. and Zhang, J. Z.: Determination of dissolved nutrients (N, P, Si)  
931 in seawater with high precision and inter-comparability using gas-segmented  
932 continuous flow analysers, *Go-sh. Repeat Hydrogr. Man. IOCCP Rep. A Collect.*  
933 *Expert Reports Guidel.*, 134(14), 1–87 [online] Available from:  
934 <http://archimer.ifremer.fr/doc/00020/13141/>, 2010.

935 Janssen, D. J., Conway, T. M., John, S. G., Christian, J. R., Kramer, D. I., Pedersen,  
936 T. F. and Cullen, J. T.: Undocumented water column sink for cadmium in open ocean  
937 oxygen-deficient zones, *Proc. Natl. Acad. Sci.*, 111(19), 6888–6893,  
938 doi:10.1073/pnas.1402388111, 2014.

939 John, S. G., Helgoe, J., Townsend, E., Weber, T., DeVries, T., Tagliabue, A., Moore,  
940 K., Lam, P., Marsay, C. M. and Till, C.: Biogeochemical cycling of Fe and Fe stable  
941 isotopes in the Eastern Tropical South Pacific, *Mar. Chem.*, 201(March), 66–76,  
942 doi:10.1016/j.marchem.2017.06.003, 2018.

943 Karstensen, J., Stramma, L. and Visbeck, M.: Oxygen minimum zones in the eastern  
944 tropical Atlantic and Pacific oceans, *Prog. Oceanogr.*, 77(4), 331–350,  
945 doi:10.1016/j.pocean.2007.05.009, 2008.

946 Keeling, R. F., Körtzinger, A. and Gruber, N.: Ocean Deoxygenation in a Warming  
947 World, *Ann. Rev. Mar. Sci.*, 2(1), 199–229,  
948 doi:10.1146/annurev.marine.010908.163855, 2010.

949 Klar, J. K., Schlosser, C., Milton, J. A., Woodward, E. M. S., Lacan, F., Parkinson, I.  
950 J., Achterberg, E. P. and James, R. H.: Sources of dissolved iron to oxygen minimum  
951 zone waters on the Senegalese continental margin in the tropical North Atlantic  
952 Ocean: Insights from iron isotopes, *Geochim. Cosmochim. Acta*, 236, 60–78,

953 doi:10.1016/j.gca.2018.02.031, 2018.

954 Klinkhammer, G., Heggie, D. T. and Graham, D. W.: Metal diagenesis in oxic marine  
955 sediments, *Earth Planet. Sci. Lett.*, 61(2), 211–219, doi:10.1016/0012-  
956 821X(82)90054-1, 1982.

957 Klueglein, N. and Kappler, A.: Abiotic oxidation of Fe(II) by reactive nitrogen species  
958 in cultures of the nitrate-reducing Fe(II) oxidizer *Acidovorax* sp. BoFeN1 - questioning  
959 the existence of enzymatic Fe(II) oxidation, *Geobiology*, 11(2), 180–190,  
960 doi:10.1111/gbi.12019, 2013.

961 Lam, P. and Kuypers, M. M. M.: Microbial Nitrogen Cycling Processes in Oxygen  
962 Minimum Zones, *Ann. Rev. Mar. Sci.*, 3(1), 317–345, doi:10.1146/annurev-marine-  
963 120709-142814, 2011.

964 Lam, P., Lavik, G., Jensen, M. M., van de Vossenberg, J., Schmid, M., Woebken, D.,  
965 Gutierrez, D., Amann, R., Jetten, M. S. M. and Kuypers, M. M. M.: Revising the  
966 nitrogen cycle in the Peruvian oxygen minimum zone, *Proc. Natl. Acad. Sci.*, 106(12),  
967 4752–4757, doi:10.1073/pnas.0812444106, 2009.

968 Lane, T. W. and Morel, F. M. M.: A biological function for cadmium in marine diatoms,  
969 *Proc. Natl. Acad. Sci.*, 97(9), 4627–4631, doi:10.1073/pnas.090091397, 2000.

970 Lee, J. and Morel, F.: Replacement of zinc by cadmium in marine phytoplankton,  
971 *Mar. Ecol. Prog. Ser.*, 127(1–3), 305–309, doi:10.3354/meps127305, 1995.

972 Lenstra, W. K., Hermans, M., Séguret, M. J. M., Witbaard, R., Behrends, T., Dijkstra,  
973 N., van Helmond, N. A. G. M., Kraal, P., Laan, P., Rijkenberg, M. J. A., Severmann,  
974 S., Teacă, A. and Slomp, C. P.: The shelf-to-basin iron shuttle in the Black Sea  
975 revisited, *Chem. Geol.*, 511(April), 314–341, doi:10.1016/j.chemgeo.2018.10.024,  
976 2019.

977 Levin, L., Gutiérrez, D., Rathburn, A., Neira, C., Sellanes, J., Muñoz, P., Gallardo, V.  
978 and Salamanca, M.: Benthic processes on the Peru margin: a transect across the  
979 oxygen minimum zone during the 1997–98 El Niño, *Prog. Oceanogr.*, 53(1), 1–27,  
980 doi:10.1016/S0079-6611(02)00022-8, 2002.

981 Li, Y.-H. and Gregory, S.: Diffusion of ions in sea water and in deep-sea sediments,  
982 *Geochim. Cosmochim. Acta*, 38(5), 703–714, doi:10.1016/0016-7037(74)90145-8,  
983 1974.



984 Little, S. H., Vance, D., Lyons, T. W. and McManus, J.: Controls on trace metal  
985 authigenic enrichment in reducing sediments: Insights from modern oxygen-deficient  
986 settings, *Am. J. Sci.*, 315(2), 77–119, doi:10.2475/02.2015.01, 2015.

987 Liu, X. and Millero, F. J.: The solubility of iron in seawater, *Mar. Chem.*, 77(1), 43–54,  
988 doi:10.1016/S0304-4203(01)00074-3, 2002.

989 Lohan, M. C. and Bruland, K. W.: Elevated Fe(II) and dissolved Fe in hypoxic shelf  
990 waters off Oregon and Washington: An enhanced source of iron to coastal upwelling  
991 regimes, *Environ. Sci. Technol.*, 42(17), 6462–6468, doi:10.1021/es800144j, 2008.

992 Metzger, E., Simonucci, C., Viollier, E., Sarazin, G., Prévot, F., Elbaz-Poulichet, F.,  
993 Seidel, J.-L. and Jézéquel, D.: Influence of diagenetic processes in Thau lagoon on  
994 cadmium behavior and benthic fluxes, *Estuar. Coast. Shelf Sci.*, 72(3), 497–510,  
995 doi:10.1016/j.ecss.2006.11.016, 2007.

996 Moore, C. M., Mills, M. M., Arrigo, K. R., Berman-Frank, I., Bopp, L., Boyd, P. W.,  
997 Galbraith, E. D., Geider, R. J., Guieu, C., Jaccard, S. L., Jickells, T. D., La Roche, J.,  
998 Lenton, T. M., Mahowald, N. M., Marañón, E., Marinov, I., Moore, J. K., Nakatsuka,  
999 T., Oschlies, A., Saito, M. A., Thingstad, T. F., Tsuda, A. and Ulloa, O.: Processes  
1000 and patterns of oceanic nutrient limitation, *Nat. Geosci.*, 6(9), 701–710,  
1001 doi:10.1038/ngeo1765, 2013.

1002 Morel, F. M. M., Milligan, A. J. and Saito, M. A.: Marine Bioinorganic Chemistry: The  
1003 Role of Trace Metals in the Oceanic Cycles of Major Nutrients, in *Treatise on*  
1004 *Geochemistry*, vol. 197, pp. 123–150, Elsevier., 2014.

1005 Morse, J. W. and Luther, G. W.: Chemical influences on trace metal-sulfide  
1006 interactions in anoxic sediments, *Geochim. Cosmochim. Acta*, 63(19–20), 3373–  
1007 3378, doi:10.1016/S0016-7037(99)00258-6, 1999.

1008 Muñoz, P., Dezileau, L., Cardenas, L., Sellanes, J., Lange, C. B., Inostroza, J.,  
1009 Muratli, J. and Salamanca, M. A.: Geochemistry of trace metals in shelf sediments  
1010 affected by seasonal and permanent low oxygen conditions off central Chile, SE  
1011 Pacific (~36°S), *Cont. Shelf Res.*, 33, 51–68, doi:10.1016/j.csr.2011.11.006, 2012.

1012 Noble, A. E., Lamborg, C. H., Ohnemus, D. C., Lam, P. J., Goepfert, T. J., Measures,  
1013 C. I., Frame, C. H., Casciotti, K. L., DiTullio, G. R., Jennings, J. and Saito, M. A.:  
1014 Basin-scale inputs of cobalt, iron, and manganese from the Benguela-Angola front to

1015 the South Atlantic Ocean, *Limnol. Oceanogr.*, 57(4), 989–1010,  
1016 doi:10.4319/lo.2012.57.4.0989, 2012.

1017 Noffke, A., Hensen, C., Sommer, S., Scholz, F., Bohlen, L., Mosch, T., Graco, M. and  
1018 Wallmann, K.: Benthic iron and phosphorus fluxes across the Peruvian oxygen  
1019 minimum zone, *Limnol. Oceanogr.*, 57(3), 851–867, doi:10.4319/lo.2012.57.3.0851,  
1020 2012.

1021 Ohde, T.: Coastal Sulfur Plumes off Peru During El Niño, La Niña, and Neutral  
1022 Phases, *Geophys. Res. Lett.*, 45(14), 7075–7083, doi:10.1029/2018GL077618, 2018.

1023 Olson, L., Quinn, K. A., Siebecker, M. G., Luther, G. W., Hastings, D. and Morford, J.  
1024 L.: Trace metal diagenesis in sulfidic sediments: Insights from Chesapeake Bay,  
1025 *Chem. Geol.*, 452, 47–59, doi:10.1016/j.chemgeo.2017.01.018, 2017.

1026 Oschlies, A., Schulz, K. G., Riebesell, U. and Schmittner, A.: Simulated 21st  
1027 century's increase in oceanic suboxia by CO<sub>2</sub>-enhanced biotic carbon export, *Global*  
1028 *Biogeochem. Cycles*, 22(4), 1–10, doi:10.1029/2007GB003147, 2008.

1029 Peng, Q., Xie, S.-P., Wang, D., Zheng, X.-T. and Zhang, H.: Coupled ocean-  
1030 atmosphere dynamics of the 2017 extreme coastal El Niño, *Nat. Commun.*, 10(1),  
1031 298, doi:10.1038/s41467-018-08258-8, 2019.

1032 Pennington, J. T., Mahoney, K. L., Kuwahara, V. S., Kolber, D. D., Calienes, R. and  
1033 Chavez, F. P.: Primary production in the eastern tropical Pacific: A review, *Prog.*  
1034 *Oceanogr.*, 69(2–4), 285–317, doi:10.1016/j.pocean.2006.03.012, 2006.

1035 Point, D., Monperrus, M., Tessier, E., Amouroux, D., Chauvaud, L., Thouzeau, G.,  
1036 Jean, F., Amice, E., Grall, J., Leynaert, A., Clavier, J. and Donard, O. F. X.: Biological  
1037 control of trace metal and organometal benthic fluxes in a eutrophic lagoon (Thau  
1038 Lagoon, Mediterranean Sea, France), *Estuar. Coast. Shelf Sci.*, 72(3), 457–471,  
1039 doi:10.1016/j.ecss.2006.11.013, 2007.

1040 Price, N. M. and Morel, F. M. M.: Cadmium and cobalt substitution for zinc in a  
1041 marine diatom, *Nature*, 344(6267), 658–660, doi:10.1038/344658a0, 1990.

1042 Ragueneau, O., Tréguer, P., Leynaert, A., Anderson, R. F., Brzezinski, M. A.,  
1043 DeMaster, D. J., Dugdale, R. C., Dymond, J., Fischer, G., François, R., Heinze, C.,  
1044 Maier-Reimer, E., Martin-Jézéquel, V., Nelson, D. M. and Quéguiner, B.: A review of  
1045 the Si cycle in the modern ocean: Recent progress and missing gaps in the

1046 application of biogenic opal as a paleoproductivity proxy, *Glob. Planet. Change*,  
1047 26(4), 317–365, doi:10.1016/S0921-8181(00)00052-7, 2000.

1048 Raiswell, R. and Canfield, D. E.: The Iron Biogeochemical Cycle Past and Present,  
1049 *Geochemical Perspect.*, 1(1), 1–220, doi:10.7185/geochempersp.1.1, 2012.

1050 Rapp, I., Schlosser, C., Rusiecka, D., Gledhill, M. and Achterberg, E. P.: Automated  
1051 preconcentration of Fe, Zn, Cu, Ni, Cd, Pb, Co, and Mn in seawater with analysis  
1052 using high-resolution sector field inductively-coupled plasma mass spectrometry,  
1053 *Anal. Chim. Acta*, 976, 1–13, doi:10.1016/j.aca.2017.05.008, 2017.

1054 Rapp, I., Schlosser, C., Menzel Barraqueta, J.-L., Wenzel, B., Lüdke, J., Scholten, J.,  
1055 Gasser, B., Reichert, P., Gledhill, M., Dengler, M. and Achterberg, E. P.: Controls on  
1056 redox-sensitive trace metals in the Mauritanian oxygen minimum zone,  
1057 *Biogeosciences Discuss.*, (November), 1–49, doi:10.5194/bg-2018-472, 2018.

1058 Rickard, D., Griffith, A., Oldroyd, A., Butler, I. B., Lopez-Capel, E., Manning, D. A. C.  
1059 and Apperley, D. C.: The composition of nanoparticulate mackinawite, tetragonal  
1060 iron(II) monosulfide, *Chem. Geol.*, 235(3–4), 286–298,  
1061 doi:10.1016/j.chemgeo.2006.07.004, 2006.

1062 Rigaud, S., Radakovitch, O., Couture, R. M., Deflandre, B., Cossa, D., Garnier, C.  
1063 and Garnier, J. M.: Mobility and fluxes of trace elements and nutrients at the  
1064 sediment-water interface of a lagoon under contrasting water column oxygenation  
1065 conditions, *Appl. Geochemistry*, 31(April 2013), 35–51,  
1066 doi:10.1016/j.apgeochem.2012.12.003, 2013.

1067 Rosenthal, Y., Lam, P., Boyle, E. A. and Thomson, J.: Precipitation and  
1068 postdepositional mobility, *Earth Planet. Sci. Lett.*, 132, 99–111, doi:10.1016/0012-  
1069 821X(95)00056-I, 1995.

1070 Rue, E. L. and Bruland, K. W.: The role of organic complexation on ambient iron  
1071 chemistry in the equatorial Pacific Ocean and the response of a mesoscale iron  
1072 addition experiment, *Limnol. Oceanogr.*, 42(5), 901–910,  
1073 doi:10.4319/lo.1997.42.5.0901, 1997.

1074 Saito, M. A., Goepfert, T. J. and Ritt, J. T.: Some thoughts on the concept of  
1075 colimitation: Three definitions and the importance of bioavailability, *Limnol.*  
1076 *Oceanogr.*, 53(1), 276–290, doi:10.4319/lo.2008.53.1.0276, 2008.

1077 Schlosser, C., Streu, P., Frank, M., Lavik, G., Croot, P. L., Dengler, M. and  
1078 Achterberg, E. P.: H<sub>2</sub>S events in the Peruvian oxygen minimum zone facilitate  
1079 enhanced dissolved Fe concentrations, *Sci. Rep.*, 8(1), 1–8, doi:10.1038/s41598-  
1080 018-30580-w, 2018.

1081 Schmidtko, S., Stramma, L. and Visbeck, M.: Decline in global oceanic oxygen  
1082 content during the past five decades, *Nature*, 542(7641), 335–339,  
1083 doi:10.1038/nature21399, 2017.

1084 Scholz, F. and Neumann, T.: Trace element diagenesis in pyrite-rich sediments of the  
1085 Achterwasser lagoon, SW Baltic Sea, *Mar. Chem.*, 107(4), 516–532,  
1086 doi:10.1016/j.marchem.2007.08.005, 2007.

1087 Scholz, F., Mcmanus, J., Mix, A. C., Hensen, C. and Schneider, R. R.: The impact of  
1088 ocean deoxygenation on iron release from continental margin sediments, *Nat.*  
1089 *Geosci.*, 7(6), 433–437, doi:10.1038/ngeo2162, 2014.

1090 Scholz, F., Löscher, C. R., Fiskal, A., Sommer, S., Hensen, C., Lomnitz, U., Wuttig,  
1091 K., Göttlicher, J., Kossel, E., Steininger, R. and Canfield, D. E.: Nitrate-dependent  
1092 iron oxidation limits iron transport in anoxic ocean regions, *Earth Planet. Sci. Lett.*,  
1093 454, 272–281, doi:10.1016/j.epsl.2016.09.025, 2016.

1094 Schunck, H., Lavik, G., Desai, D. K., Großkopf, T., Kalvelage, T., Löscher, C. R.,  
1095 Paulmier, A., Contreras, S., Siegel, H., Holtappels, M., Rosenstiel, P., Schilhabel, M.  
1096 B., Graco, M., Schmitz, R. A., Kuypers, M. M. M. and LaRoche, J.: Giant Hydrogen  
1097 Sulfide Plume in the Oxygen Minimum Zone off Peru Supports  
1098 Chemolithoautotrophy, *PLoS One*, 8(8), doi:10.1371/journal.pone.0068661, 2013.

1099 Scor Working Group: GEOTRACES – An international study of the global marine  
1100 biogeochemical cycles of trace elements and their isotopes, *Geochemistry*, 67(2),  
1101 85–131, doi:10.1016/j.chemer.2007.02.001, 2007.

1102 Severmann, S., McManus, J., Berelson, W. M. and Hammond, D. E.: The continental  
1103 shelf benthic iron flux and its isotope composition, *Geochim. Cosmochim. Acta*,  
1104 74(14), 3984–4004, doi:10.1016/j.gca.2010.04.022, 2010.

1105 Shibamoto, Y. and Harada, K.: Silicon flux and distribution of biogenic silica in deep-  
1106 sea sediments in the western North Pacific Ocean, *Deep Sea Res. Part I Oceanogr.*  
1107 *Res. Pap.*, 57(2), 163–174, doi:10.1016/j.dsr.2009.10.009, 2010.

1108 Sommer, S., Linke, P., Pfannkuche, O., Schleicher, T., Schneider v. D, D., Reitz, A.,  
1109 Haeckel, M., Flögel, S. and Hensen, C.: Seabed methane emissions and the habitat  
1110 of frenulate tubeworms on the Captain Arutyunov mud volcano (Gulf of Cadiz), *Mar.*  
1111 *Ecol. Prog. Ser.*, 382, 69–86, doi:10.3354/meps07956, 2009.

1112 Sommer, S., Gier, J., Treude, T., Lomnitz, U., Dengler, M., Cardich, J. and Dale, A.  
1113 W.: Depletion of oxygen, nitrate and nitrite in the Peruvian oxygen minimum zone  
1114 cause an imbalance of benthic nitrogen fluxes, *Deep. Res. Part I Oceanogr. Res.*  
1115 *Pap.*, 112(3), 113–122, doi:10.1016/j.dsr.2016.03.001, 2016.

1116 Stookey, L. L.: Ferrozine---a new spectrophotometric reagent for iron, *Anal. Chem.*,  
1117 42(7), 779–781, doi:10.1021/ac60289a016, 1970.

1118 Stramma, L., Johnson, G. C., Sprintall, J. and Mohrholz, V.: Expanding Oxygen-  
1119 Minimum Zones in the Tropical Oceans, *Science (80-. )*, 320(5876), 655–658,  
1120 doi:10.1126/science.1153847, 2008.

1121 Stramma, L., Schmidtko, S., Levin, L. A. and Johnson, G. C.: Ocean oxygen minima  
1122 expansions and their biological impacts, *Deep. Res. Part I Oceanogr. Res. Pap.*,  
1123 57(4), 587–595, doi:10.1016/j.dsr.2010.01.005, 2010.

1124 Straub, K. L., Benz, M., Schink, B. and Widdel, F.: Anaerobic, nitrate-dependent  
1125 microbial oxidation of ferrous iron. *Appl Environ Microbiol*, *Appl. Environ. Microbiol.*,  
1126 62(4), 1458–60, 1996.

1127 Sunda, W. G. and Huntsman, S. A.: Effect of Zn, Mn, and Fe on Cd accumulation in  
1128 phytoplankton: Implications for oceanic Cd cycling, *Limnol. Oceanogr.*, 45(7), 1501–  
1129 1516, doi:10.4319/lo.2000.45.7.1501, 2000.

1130 Sundby, B., Martinez, P. and Gobeil, C.: Comparative geochemistry of cadmium,  
1131 rhenium, uranium, and molybdenum in continental margin sediments, *Geochim.*  
1132 *Cosmochim. Acta*, 68(11), 2485–2493, doi:10.1016/j.gca.2003.08.011, 2004.

1133 Taylor, S. R. and McLennan, S. M.: Planetary crusts: Their composition, origin and  
1134 evolution , by Stuart Ross Taylor and Scott M. McLennan, *Meteorit. Planet. Sci.*,  
1135 44(3), 465–466, doi:10.1111/j.1945-5100.2009.tb00744.x, 2009.

1136 Thamdrup, B., Dalsgaard, T. and Revsbech, N. P.: Widespread functional anoxia in  
1137 the oxygen minimum zone of the Eastern South Pacific, *Deep Sea Res. Part I*  
1138 *Oceanogr. Res. Pap.*, 65, 36–45, doi:10.1016/j.dsr.2012.03.001, 2012.

1139 Turetta, C., Capodaglio, G., Cairns, W., Rabar, S. and Cescon, P.: Benthic fluxes of  
1140 trace metals in the lagoon of Venice, *Microchem. J.*, 79(1–2), 149–158,  
1141 doi:10.1016/j.microc.2004.06.003, 2005.

1142 Twining, B. S. and Baines, S. B.: The Trace Metal Composition of Marine  
1143 Phytoplankton, *Ann. Rev. Mar. Sci.*, 5(1), 191–215, doi:10.1146/annurev-marine-  
1144 121211-172322, 2013.

1145 Vedamati, J., Goepfert, T. and Moffett, J. W.: Iron speciation in the eastern tropical  
1146 south pacific oxygen minimum zone off peru, *Limnol. Oceanogr.*, 59(6), 1945–1957,  
1147 doi:10.4319/lo.2014.59.6.1945, 2014.

1148 Westerlund, S. F. G., Anderson, L. G., Hall, P. O. J., Iverfeldt, Å., Van Der Loeff, M.  
1149 M. R. and Sundby, B.: Benthic fluxes of cadmium, copper, nickel, zinc and lead in the  
1150 coastal environment, *Geochim. Cosmochim. Acta*, 50(6), 1289–1296,  
1151 doi:10.1016/0016-7037(86)90412-6, 1986.

1152 Xie, R. C., Rehkämper, M., Grasse, P., van de Flierdt, T., Frank, M. and Xue, Z.:  
1153 Isotopic evidence for complex biogeochemical cycling of Cd in the eastern tropical  
1154 South Pacific, *Earth Planet. Sci. Lett.*, 512, 134–146, doi:10.1016/j.epsl.2019.02.001,  
1155 2019.

1156 Xu, Y., Feng, L., Jeffrey, P. D., Shi, Y. and Morel, F. M. M.: Structure and metal  
1157 exchange in the cadmium carbonic anhydrase of marine diatoms, *Nature*, 452(7183),  
1158 56–61, doi:10.1038/nature06636, 2008.

1159 Yücel, M., Sommer, S., Dale, A. W. and Pfannkuche, O.: Microbial sulfide filter along  
1160 a benthic redox gradient in the Eastern Gotland Basin, Baltic Sea, *Front. Microbiol.*,  
1161 8(FEB), 1–16, doi:10.3389/fmicb.2017.00169, 2017.

1162 Zago, C., Capodaglio, G., Ceradini, S., Ciceri, G., Abemoschi, L., Soggia, F.,  
1163 Cescon, P. and Scarponi, G.: Benthic fluxes of cadmium, lead, copper and nitrogen  
1164 species in the northern Adriatic Sea in front of the River Po outflow, Italy, *Sci. Total*  
1165 *Environ.*, 246(2–3), 121–137, doi:10.1016/S0048-9697(99)00421-0, 2000.

1166 Zumft, W. G.: Cell biology and molecular basis of denitrification., *Microbiol. Mol. Biol.*  
1167 *Rev.*, 61(4), 533–616 [online] Available from:  
1168 <http://www.ncbi.nlm.nih.gov/pubmed/9409151>  
1169 <http://www.pubmedcentral.nih.gov/articlerender.fcgi?artid=PMC232623>, 1997.

1171 **Figure captions**

1172

1173 Fig. 1: Sampling stations on the Peruvian continental margin during cruises M136 &  
1174 M137 along a latitudinal depth transect at 12° S. The sampling stations for pore  
1175 waters are depicted by white stars, for bottom waters by yellow dots and for benthic  
1176 chamber incubations by red dots.

1177 Fig. 2: Oxygen, nitrate, nitrite and hydrogen sulfide concentrations on the Peruvian  
1178 slope (Station 10, 1000 m depth), crossing the oxygen minimum zone (upper panel),  
1179 and the upper shelf (Station 1, 75 m depth) (lower panel) during cruises M136 &  
1180 M137 and M92 along the 12° S transect.

1181 Fig. 3: Near-bottom water concentrations of dissolved Fe and Cd and dissolved Fe to  
1182 silicic acid ratios 0.5 m to 4 m above the seafloor across the 12° S transect. The red  
1183 diamonds show results from a second sampling at Station 1 one month later.  
1184 Concentrations of silicic acid are listed in Table S3 in the supplement.

1185 Fig. 4: Pore water dissolved Fe(II) and hydrogen sulfide concentrations. Data from  
1186 an earlier cruise, M92, at Station 1 (75 m water depth) are displayed for comparison.  
1187 The uppermost sample represents the bottom water concentration. The analytical  
1188 error is smaller than the symbol size.

1189 Fig. 5: Dissolved Fe concentrations in incubated bottom waters from benthic chamber  
1190 incubations. The grey dashed line represents the linear regressions of the  
1191 concentration change over the incubation time. The equations for these linear  
1192 regressions are listed together with the coefficients of determination ( $R^2$ ) in Table S4  
1193 in the supplement. The black dashed line represents theoretical concentration  
1194 gradients over the incubation time based on our benthic diffusive fluxes (Table 2).  
1195 The analytical error is smaller than the symbol size.

1196 Fig. 6: Pore water dissolved Cd and hydrogen sulfide concentrations. The uppermost  
1197 sample represents the bottom water concentrations. The analytical error is smaller  
1198 than the symbol size.

1199 Fig. 7: Dissolved Cd concentrations in incubated bottom waters from benthic  
1200 chamber incubations. The grey dashed line represents the linear regressions of the  
1201 concentration change over the incubation time. The equations for these linear

1202 regressions are listed together with the coefficients of determination ( $R^2$ ) in Table S4  
1203 in the supplement. The black dashed line represents theoretical concentration  
1204 gradients over the incubation time based on our benthic diffusive fluxes (Table 3).  
1205 The analytical error is smaller than the symbol size.

1206 Fig. 8: Dissolved Fe, nitrate and nitrite concentrations in incubated bottom waters  
1207 from the benthic chamber incubation at Station 4 (145 m water depth).

1208 Fig. 9: Comparison of benthic diffusive Fe(II) fluxes between cruises M136 & M137  
1209 and M92 on the Peruvian shelf. Negative values represent fluxes from the sediment  
1210 pore water into the bottom waters. Shaded bars on the upper panel display the  
1211 geochemical conditions in the water column during the time of sampling.

1212 Fig. 10: Schematic overview of the possible mobility of different trace metal to an  
1213 expansion of sulfidic conditions. Saturation indices (SI) were calculated for different  
1214  $H_2S$  concentrations and reported minimum and maximum concentrations of trace  
1215 metals in the water column (data from Bruland and Lohan 2003). Equilibrium  
1216 constants ( $\log K$  under standard conditions) for Fe (FeS ppt: -3.92), Ni (millerite: -  
1217 8.04), Zn (sphalerite: -11.62) and Cd (greenokite: -15.93) were taken from the  
1218 PHREEQC WATEQ4F database (Ball and Nordstrom, 1991). The results are  
1219 approximate since concentrations instead of activities were used for calculations. A  
1220 positive SI is indicative of oversaturation whereas a negative SI is indicative of  
1221 undersaturation.



1222 Table 1: Accuracy of replicate concentration measurements (n = 7) of certified  
 1223 reference seawater for trace metals NASS-7 and CASS-6 by ICP-MS.

	NASS-7 certified value	NASS-7 measured value	CASS-6 certified value	CASS-6 measured value
Fe (µg/L)	0.351 ± 0.026	0.352 ± 0.017	1.56 ± 0.12	1.56 ± 0.03
Cd (µg/L)	0.0161 ± 0.0016	0.0162 ± 0,0024	0.0217 ± 0.0018	0.0216 ± 0.0016

1224

1225

1226 Table 2: Comparison of benthic diffusive Fe(II) fluxes out of the sediment and  
 1227 geochemical bottom water conditions between M136 & M137 and M92 on the  
 1228 Peruvian shelf. Fluxes during M92 correspond to similar depth (see Fig. 9).

station	M136 & M137	M136 & M137	M136 & M137	M136 & M137	M136 & M137	M136 & M137	M92	M92
	water depth	latitude	longitude	water column condition	Fe(II) flux diffusive	Fe flux benthic chamber	water column condition	Fe(II) flux diffusive
	(m)	(S)	(W)		(mmol m <sup>-2</sup> y <sup>-1</sup> )	(mmol m <sup>-2</sup> y <sup>-1</sup> )		(mmol m <sup>-2</sup> y <sup>-1</sup> )
1	75	12°13.52	77°10.93	O <sub>2</sub> < 5 µM	-2.56	-1.74	slightly sulfidic	-22.69
3	130	12°16.68	77°14.95	nitrogenous	-0.81	-	slightly sulfidic	-3.16
4	145	12°18.71	77°17.80	nitrogenous	-17.45	-8,57	nitrogenous	-5.77
5	195	12°21.50	77°21.70	nitrogenous	-2.49	2.01	nitrogenous	-1.51
6	245	12°23.30	77°24.82	nitrogenous	-7.96	-5,43	nitrogenous	-10.20
9	750	12°31.35	77°35.01	O <sub>2</sub> > 5 µM	0.00	-6.11	O <sub>2</sub> > 5 µM	0.00
10	970	12°34.90	77°40.32	O <sub>2</sub> > 5 µM	-0.26	-1.68	O <sub>2</sub> > 5 µM	-0.12

1229

1230

1231

1232

1233 Table 3: Comparison of sedimentary Cd excess compared to the lithogenic  
 1234 background and the contribution of Cd delivery to the sediment via different  
 1235 pathways: (1) diffusion across the sediment-water interface and Cd sulfide  
 1236 precipitation within the sediment; (2) Cd incorporation by phytoplankton and delivery  
 1237 to the sediment with organic matter; (3) Cd sulfide precipitation in the water column  
 1238 and particulate delivery to the sediment.

station	water depth	Cd excess sediment <sup>1</sup>	(1) Cd flux diffusive	Cd flux benthic chamber	H <sub>2</sub> S in surface sediment below benthic chamber	(2) Cd from organic matter <sup>2</sup>	(3) CdS precipitation in water column <sup>3</sup>
	(m)	( $\mu\text{mol m}^{-2} \text{y}^{-1}$ )	( $\mu\text{mol m}^{-2} \text{y}^{-1}$ )	( $\mu\text{mol m}^{-2} \text{y}^{-1}$ )	( $\mu\text{M}$ )	( $\mu\text{mol m}^{-2} \text{y}^{-1}$ )	( $\mu\text{mol m}^{-2} \text{y}^{-1}$ )
1	75	248.87	-1.85	-1.6 (3109.5) <sup>4</sup>	641.02	8.34 – 49.04	199.83 – 240.53
3	130	153.41	0.83	-	-	4.87 – 17.40	135.19 – 147.72
4	145	35.07	0.54	13.4	1.30	1.55 – 6.48	28.07 – 32.99
5	195	44.76	0.63	22.6	9.52	5.71 – 7.71	36.36 – 38.36
6	245	35.15	0.55	21.2	0.40	3.60 – 6.54	28.06 – 31.00
9	750	4.44	-0.30	0	0	1.48 – 3.21	1.23 – 2.96

1239  
 1240 <sup>1</sup> Calculated after Brumsack (2006) and multiplied by the mass accumulation rate for  
 1241 each site (Dale et al., 2015b).

1242 <sup>2</sup> Determined by multiplication of Cd/C ratio in average phytoplankton (Moore et al.,  
 1243 2013) with particulate organic carbon rain rates (maximum values) and organic  
 1244 carbon accumulation rates (minimum values) for each individual site (data from Dale  
 1245 et al., 2015b).

1246 <sup>3</sup> Remainder of Cd excess in sediment after subtraction of diffusive and minimum and  
 1247 maximum organic Cd sources.

1248 <sup>4</sup> Flux calculated from the concentration difference between the bottom water (0.5 m)  
 1249 and the first sample from the benthic chamber incubation (taken after 0.25 h).

1250

1251

1252 Table 4: Modelled half-lives ( $t_{1/2}$ ) of dissolved Fe within the first 4 m distance from the  
 1253 seafloor at Stations 3 and 4 and data used for determination of  $t_{1/2}$  using Eq. (4) and  
 1254 Eq. (5).

station	water depth (m)	Si(OH) <sub>4</sub> flux benthic chamber ( $F_{Si}$ ) ( $\mu\text{mol cm}^{-2} \text{d}^{-1}$ )	Si(OH) <sub>4</sub> concentration gradient ( $d_{Si}$ ) ( $\mu\text{mol cm}^{-3} \text{cm}^{-1}$ )	eddy diffusion coefficient ( $K_y$ ) ( $\text{m}^2 \text{s}^{-1}$ )	modelled Fe at sediment surface ( $C_{BW}$ ) (nM)	Fe oxidation constant ( $k_{Feox}$ ) ( $\text{d}^{-1}$ )	half-life in near- bottom water column ( $t_{1/2}$ ) (min)
3	130	0.73	$-4.05 \cdot 10^{-6}$	$1.55 \cdot 10^6$	70	400	2.5
4	145	0.33	$-1.44 \cdot 10^{-6}$	$1.96 \cdot 10^6$	81	3500	0.3

1255

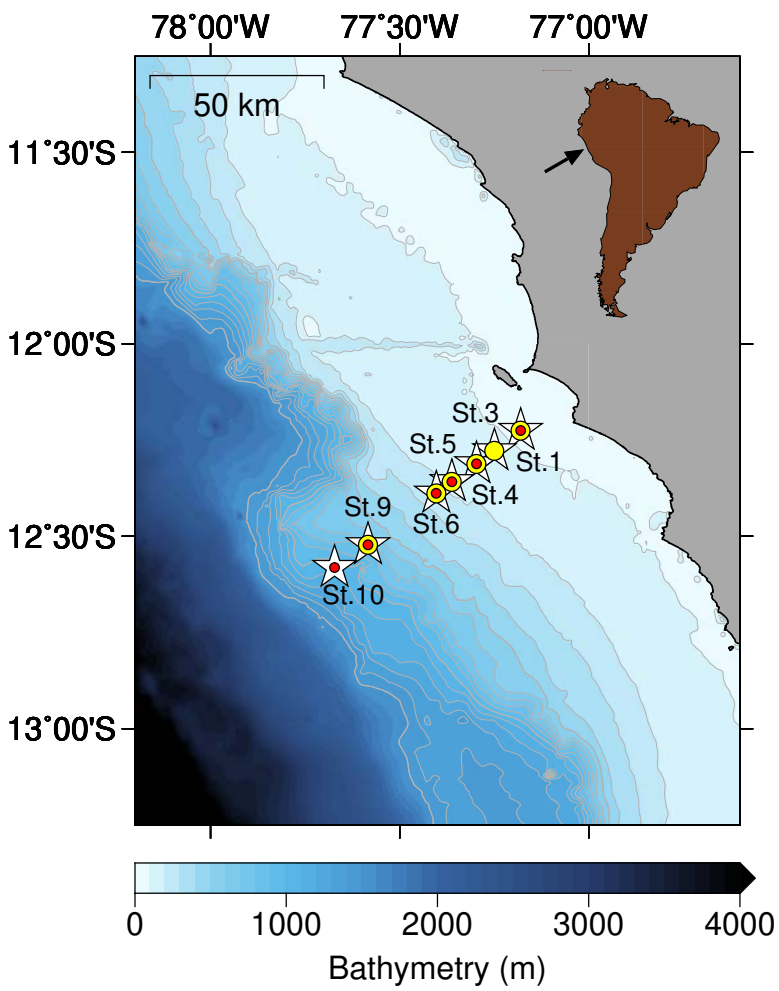


Fig. 1

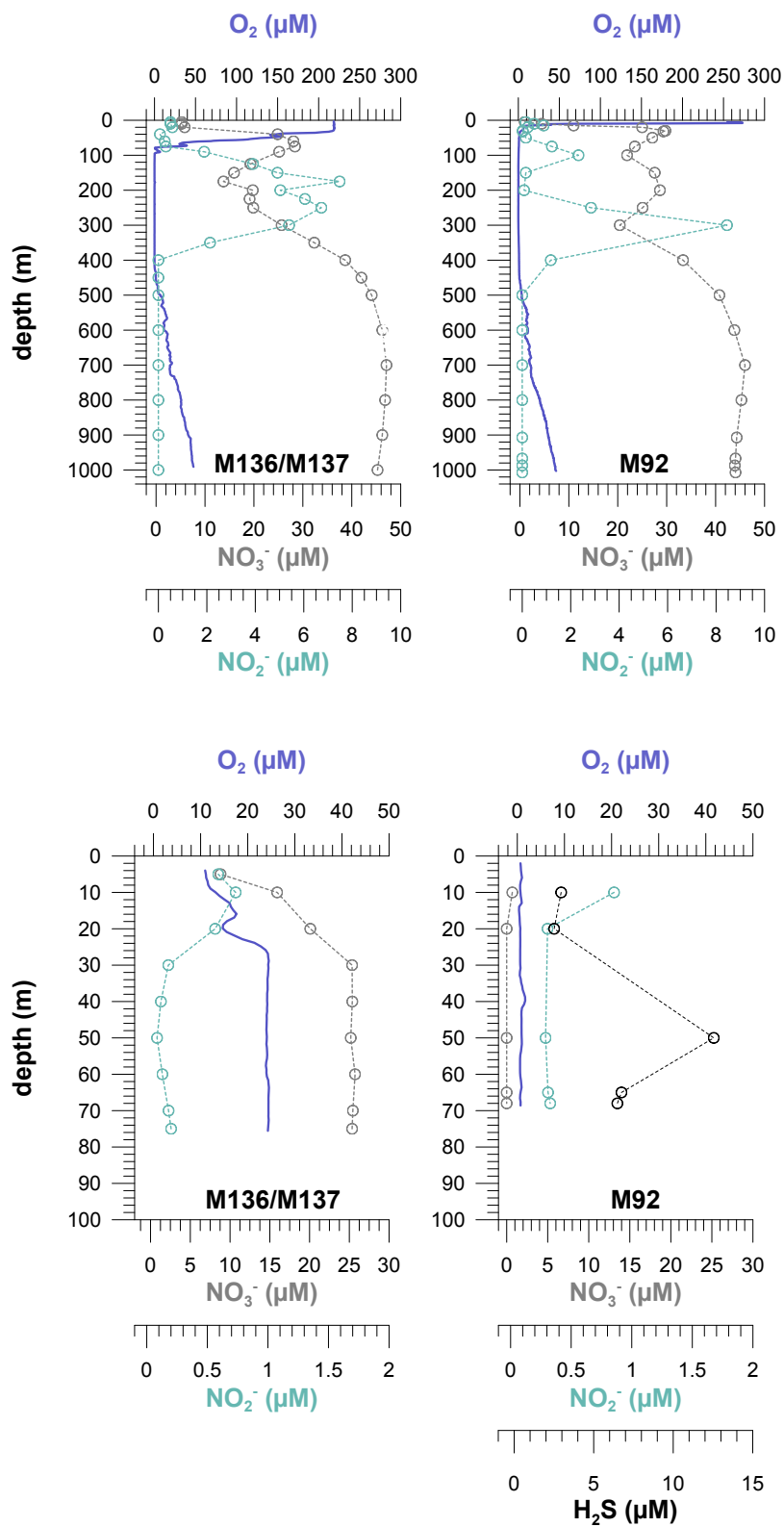


Fig. 2

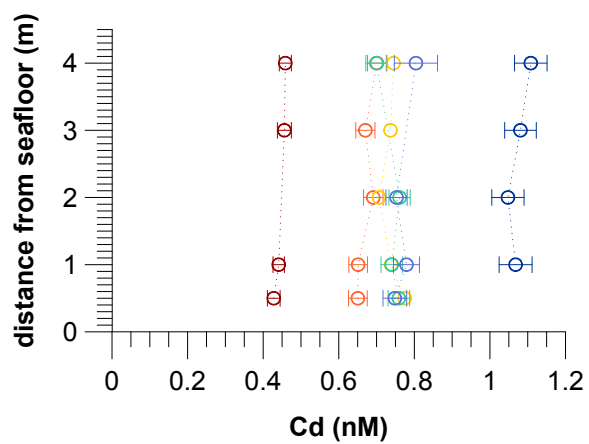
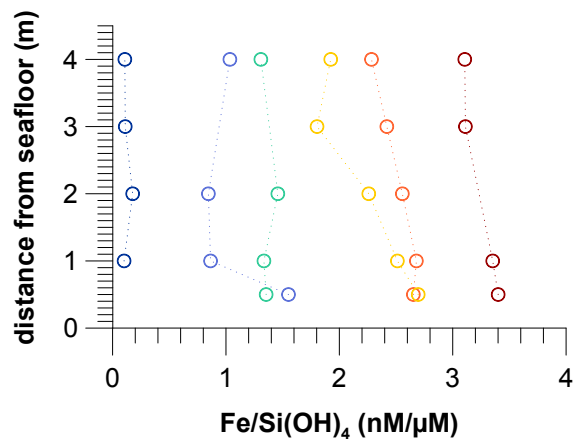
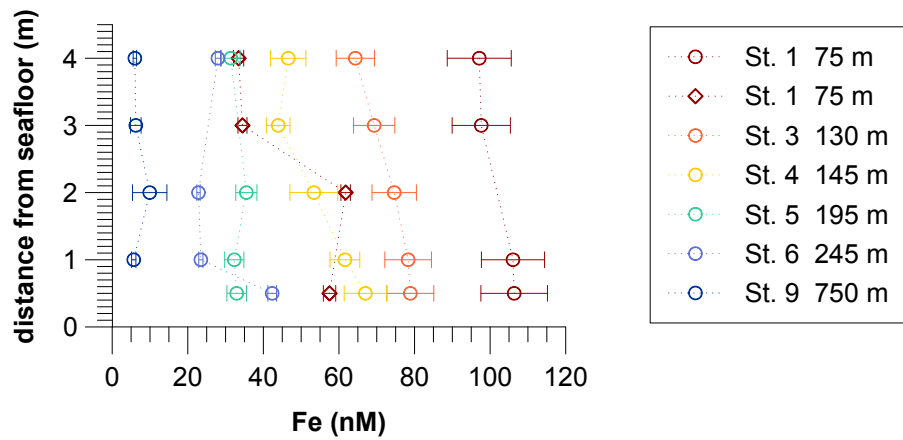


Fig. 3

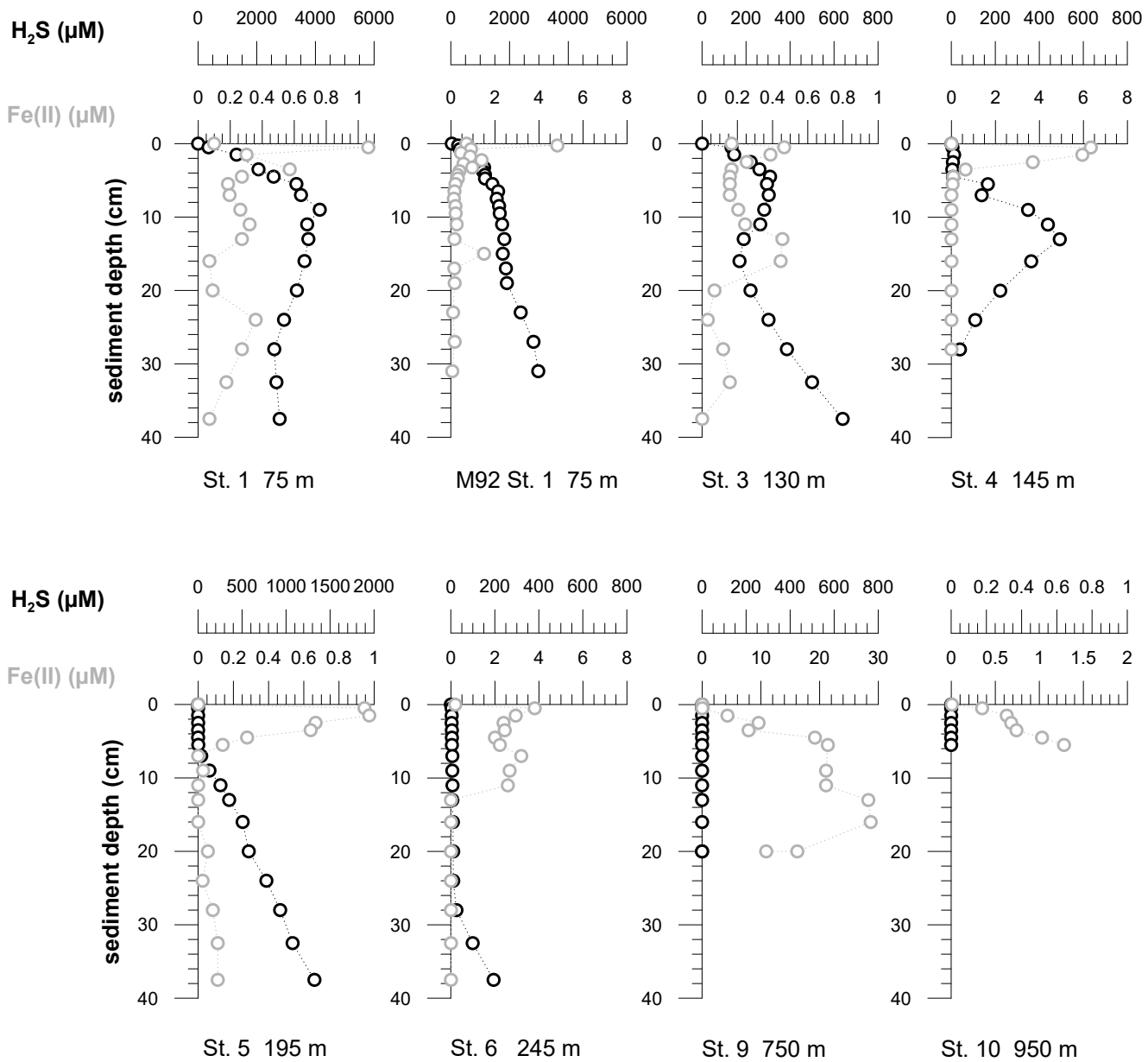


Fig. 4

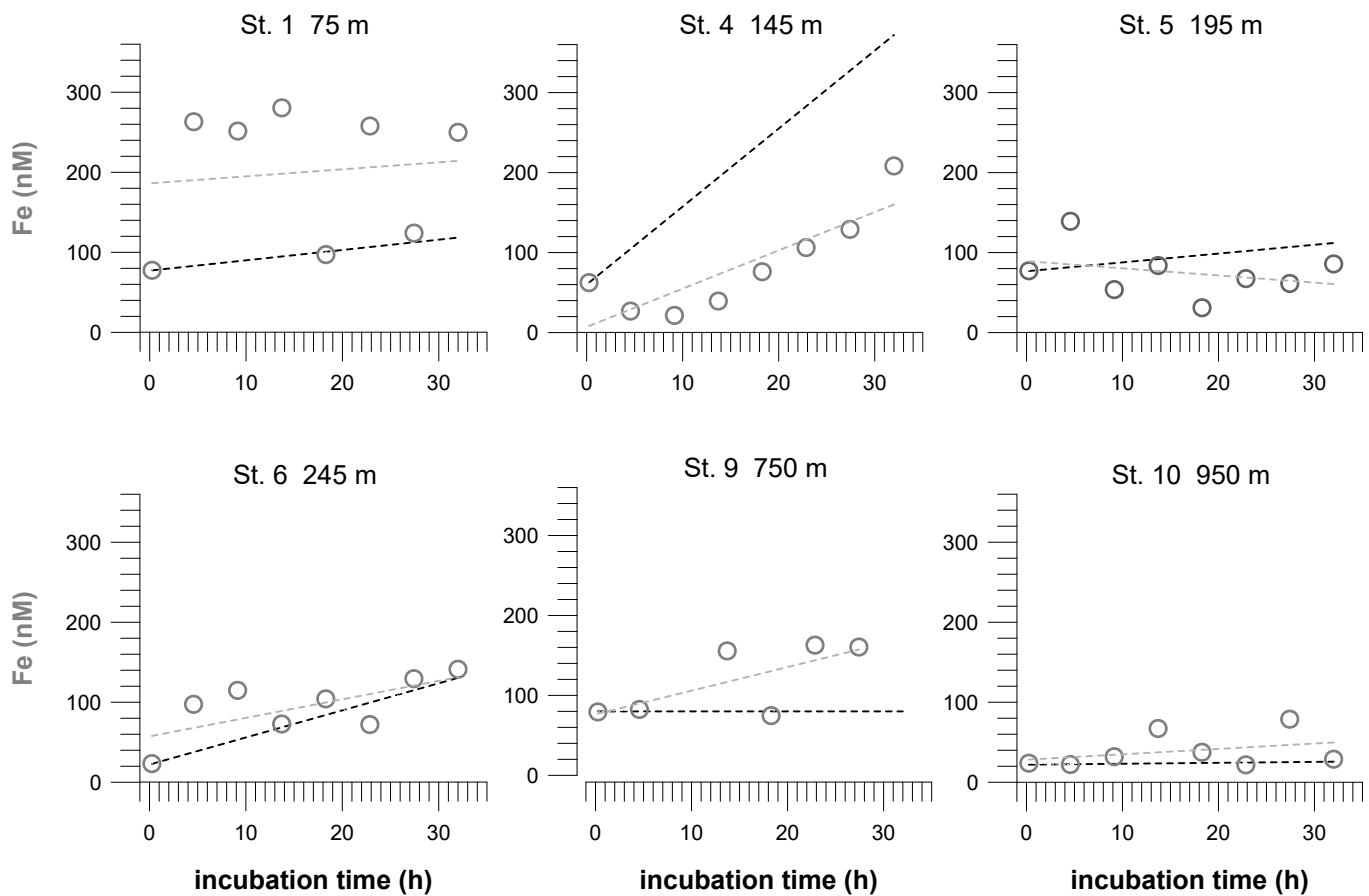


Fig. 5



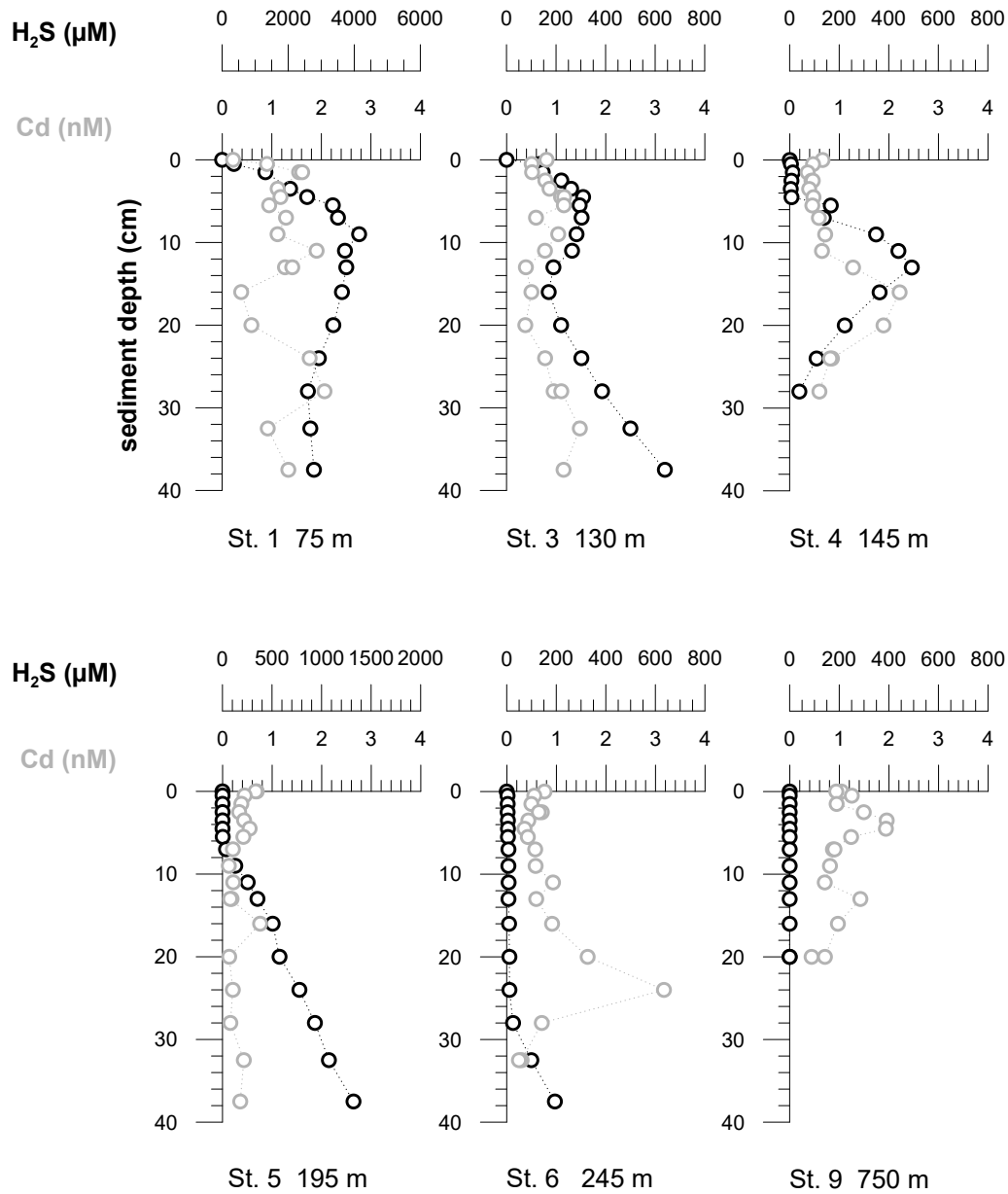


Fig. 6

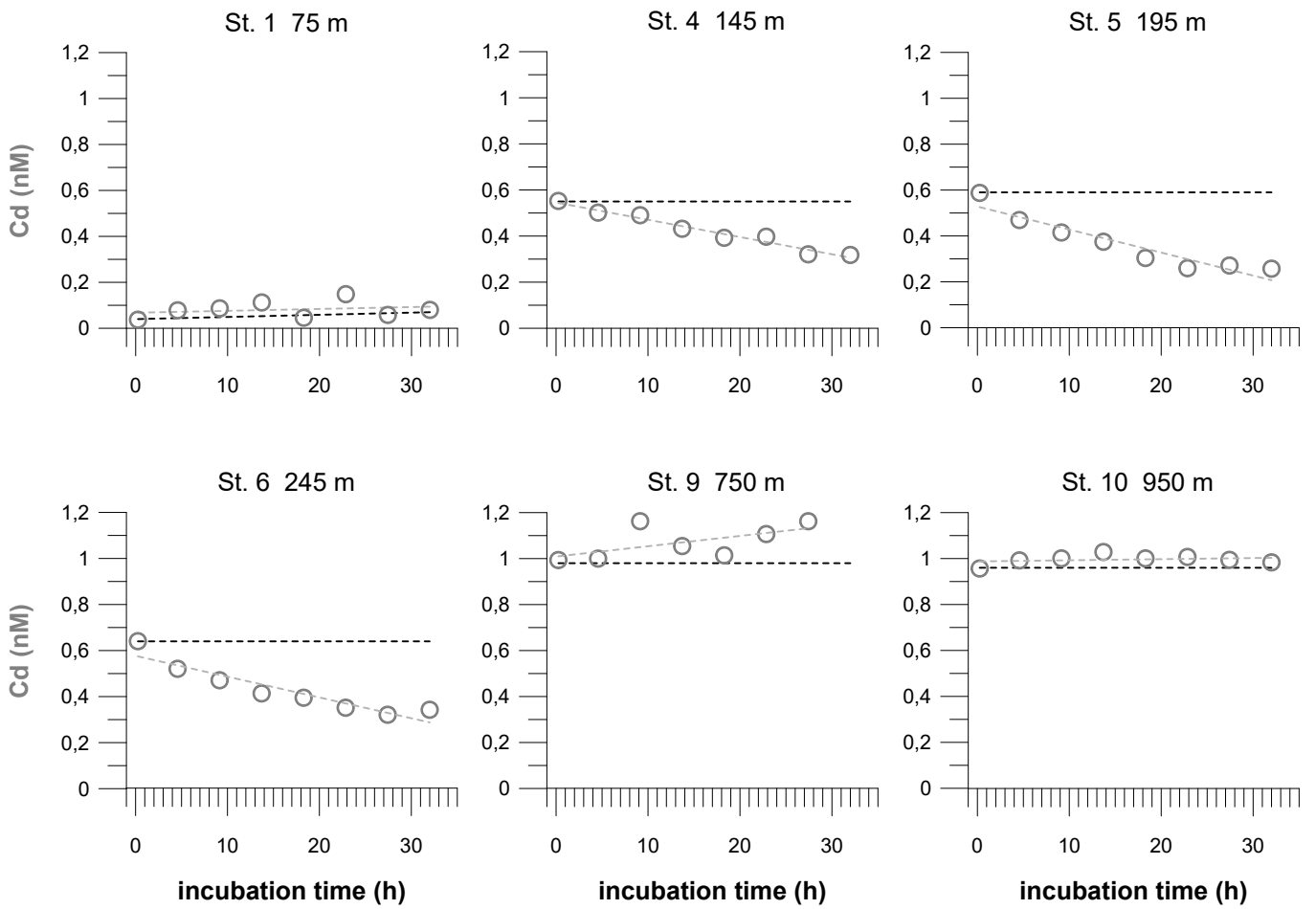


Fig. 7

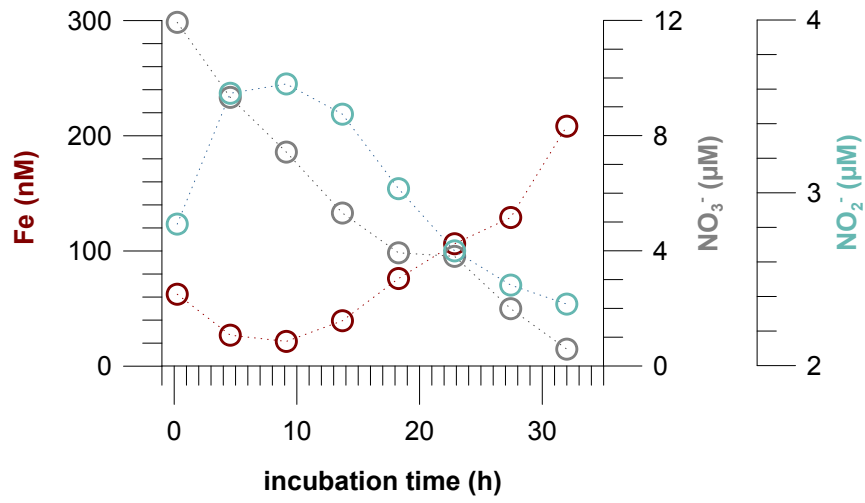


Fig. 8

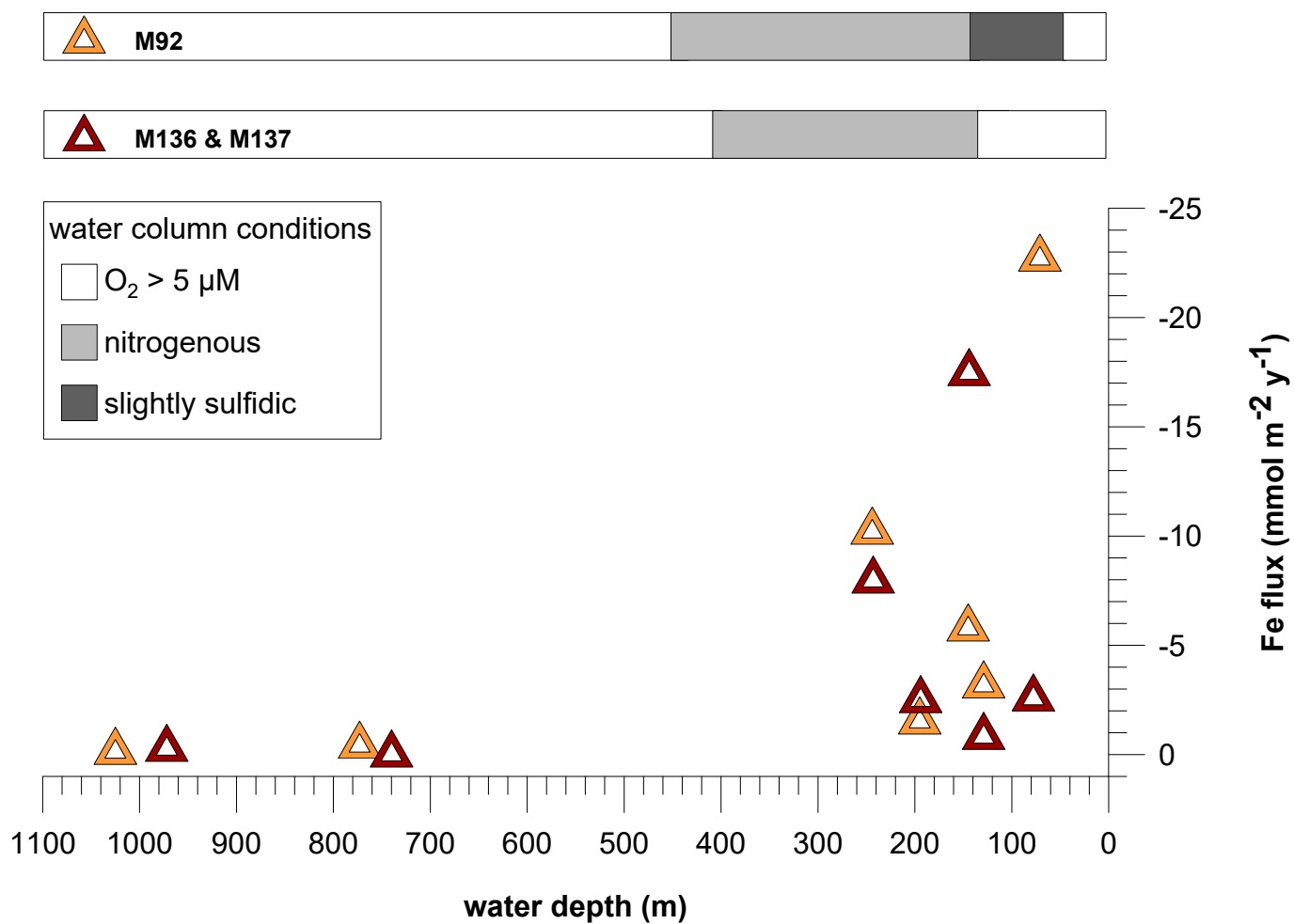


Fig. 9

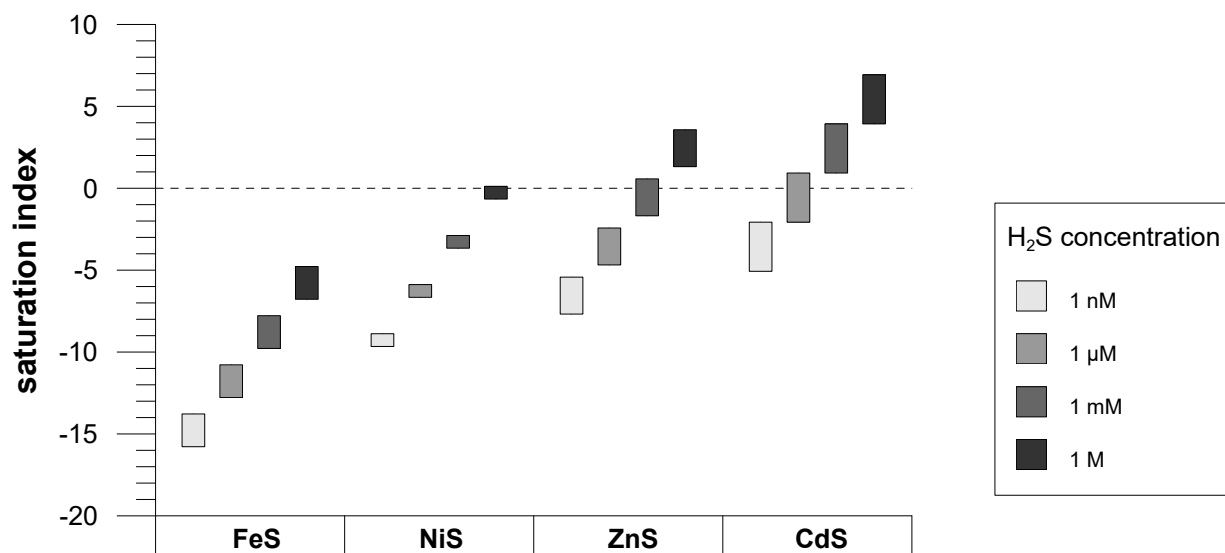


Fig. 10